Overlapping rotor design and efficient active disturbance rejection control for miniaturization of drones

March ２０２２

Heming Zhang

Overlapping rotor design and efficient active disturbance rejection control for miniaturization of drones

Graduate School of Systems and Information Engineering

University of Tsukuba

March ２０２２

Heming Zhang

Acknowledgments

Studying and researching at the University of Tsukuba has been an unforgettable time and an asset.

My supervisor, Professor Nobuhara, has guided and encouraged me from the beginning of my master's research. I learnt a lot from his humility and rigor. I am grateful to him for his dedication and guidance, which gave me the motivation to research and study. I would like to thank Professor Kawai for always giving me professional advice and help when I encountered bottlenecks in my research. I would like to thank Professor Tsubouchi, Professor Mochiyama and Professor Takayasu for reviewing and giving me comments on my research. Also, I would like to thank the members of Computational Intelligence and Multimedia Laboratory, I am glad to have studied with them.

I am grateful for the support of the Tsukuba Scholarship and Japanese Government Scholarship to help me complete my doctoral study.

Finally, I would like to express my gratitude to my parents for their understanding and support. You motivate me to do my best.

Abstract

While compact drones are popular with consumers, and more large size industrial drones are being developed to meet the needs of various industries. The development of a compact drone that combines the advantages of large and small drones is expected.

This research aims to improve the structure of conventional multi-rotor drones to create a drone that has the advantages of both small and large aircraft. We proposed a drone structure to miniaturize the multi-rotor drone without changing the rotors and propellers. The proposed structure reduces the size by shortening the distance between the motors and by making a height difference between the rotors. It is shown that the proposed 4-rotor drone (quadcopter), 6-rotor drone (hexacopter) and 8-rotor drone (octocopter) can achieve about 27%, 46% and 54% size reduction respectively compared with conventional structure.

The reduction in rotor distance leads to a reduction in rotational inertia, and the disturbance caused by downwash in the overlapping region will affect the control performance. To achieve a robust control on proposed structure, an LADRC based attitude controller with cascade structure and reduced order observer is proposed. To evaluate the proposed attitude controller, it is compared with the conventional controller in simulator and evaluated on drones.

Contents

List of Figures

List of Tables

Chapter1

Introduction

An unmanned aerial vehicle is a pilotless aircraft, which is flown without a pilot-in-command on-board and is either remotely and fully controlled from another place (ground, another aircraft, space) or programmed and fully autonomous[1].Rapid advancements in the design and development of unmanned aerial vehicles (UAVs) of different sizes, shapes and capabilities have been taking place recently with new improvements in flight control and integrated circuit technologies. These devices can enhance the operation of many environmental, commercial and military operations. Originally, UAVs were mainly used in military applications. However, the commercial drone market has observed growing demand from users across industries bringing many new valuable avenues for the commercial and usability of drones. The consumer drone market is expected to be one of the largest categories of consumer robots, and the market is growing very rapidly. Specialist consumer drones, with similar capabilities to small, low-cost commercial drones, will penetrate the toy drone sector quickly[2].
As new trends and technologies take over the market, there is an expansion phase around data driving industry growth. The commercial drone market will exceed $55 billion by 2027, according to a new study by Global Market Insights Inc[3].

1.1 Drone Applications

Drones are involved in many fields, such as investigation and rescue, monitoring of large infrastructures, transportation, and agriculture.

1.1.1 Survey and rescue applications

Search and rescue (SAR) have been a human-intensive task so far, but recent technological advancements can make it autonomous. Using drone surveillance with a recent computer vision technology can increase

the number of humans saved at the time of disaster [4].
Earthquake is a typical disaster that is broken out without any pre-sign and causing not just seriously building damages but also many human die. The chance for survive of the people trapped in collapsed buildings depends mainly on the damage types of the affected buildings. Therefore, a rapid mapping of the affected area is very important not just for assessing the damages but even more to optimize sharing our rescue sources[5]. Since the limited sources in disasters a small drone can be a good solution for rapid mapping. Floods are a typical for a slowly developing disaster. In many times authority or disaster management headquarter have enough information to predict the scale and serious of this disaster. Against the slowly developing but in many times the country large affected area citizens can be trapped. Even if manned aerials can help in these situations demonstratively, drone activity around a limited area also can help for the management[6].

1.1.2 Infrastructure inspection applications

Unmanned Aerial Vehicles have the capabilities to undertake tasks in remote, dangerous and dull situations. One of these situations is the infrastructure inspection, at which, using the UAV decreases the risk and the operation time of the task comparing to a human inspector. Together with the increasing ease of obtaining imagery, advances in computer vision and computer processing power have led to a widespread increase in aerial mapping and 3D-reconstruction[7][8][9].
Abdulla et al's research[10] presented a small vision-based UAV with the capability of inspection tasks of a civil and industrial infrastructure.
Traditionally, railway inspection and monitoring are considered a crucial aspect of the system and are done by human inspectors. Rapid progress of the machine vision-based systems enables automated and autonomous rail track detection and railway infrastructure monitoring and inspection with flexibility and ease of use. Milan et al's research[11] explored the usage of the UAVs (drones) in railways and computer vision based monitoring of railway infrastructure. Employing drones for such monitoring systems enables more robust and reliable visual inspection while providing a cost effective and accurate means for monitoring of

the tracks.

1.1.3 Agriculture applications

For years now, drone advocates have cited precision agriculture - crop management that uses GPS and big data - as a way to increase crop yield while resolving water and food crises[12].

Agricultural chemical application is frequently needed at specific times and locations for accurate site-specific management of crop pests. Piloted agricultural aircraft are typically used to treat large, unobstructed, continuous acreage crops and are not as efficient when working over small or obstructed plots. An Unmanned Aerial Vehicle (UAV), which can be remotely controlled or fly autonomously based on pre-programmed flight plans, may be used to make timely and efficient applications over these small area plots . Huang et al's research[13] developed a low volume spray system for use on a fully autonomous UAV to apply crop protection products on specified crop areas.

Obtaining accurate and timely crop height estimates is important to characterize plants' growth rate and health. Agricultural researchers use this data to measure the impact of genetic variation in the crops on drought resistance and responses to environmental stresses. David et al's research[14] presented a UAV-mounted measurement system that utilizes a laser scanner to compute crop heights, a critical indicator of crop health. The system filters, transforms, and analyzes the cluttered range data in real-time to determine the distance to the ground and to the top of the crops.

Unmanned aircraft system (UAS) is a particularly powerful tool for plant phenotyping, due to reasonable cost of procurement and deployment, ease and flexibility for control and operation, ability to reconfigure sensor payloads to diversify sensing, and the ability to seamlessly fit into a larger connected phenotyping network. These advantages have expanded the use of UAS-based plant phenotyping approach in research and breeding applications. Guo et al's research[15] reviewed the state of the art in the deployment, collection, curation, storage, and analysis of data from UAS-based phenotyping platforms.

1.2 Drone Classification

A variety of UAV system has been developed and in the advancement phase, some of them includes the Fixed-wing aircraft[16][17], helicopter[18], multirotor drone[19]. Different types of drones are used in different missions depending on their movement characteristics.

1.2.1 Fixed wing drone

Fixed wing drones are very simple but saturated in designing and manufacturing, because of successful generalization of larger fixed-wing planes with slight modifications and improvements. Fixed wings are the main lift generating elements in response to forward accelerating speed. The velocity and steeper angle of air flowing over the fixed wings controls the lift produced. Fixed wing drones require a higher initial speed and the thrust to load ratio of less than 1 to initiate a flight[20]. If fixed wing and Multirotor are compared for a same amount of payload, fixed-wing drones are more comfortable with less power requirement and thrust loading of less than 1. Rudder, ailerons and elevators are used for yaw, roll and pitch angles to control the orientation of aircraft. Fixed wing drones cannot hover at a place, and they cannot maintain their low speed. Subsequently, it can be seen that lift to drug ratio denotes the lift generated by a wing counter to drag generated. Some consumer fixed drones are shown in Fig.1-1.

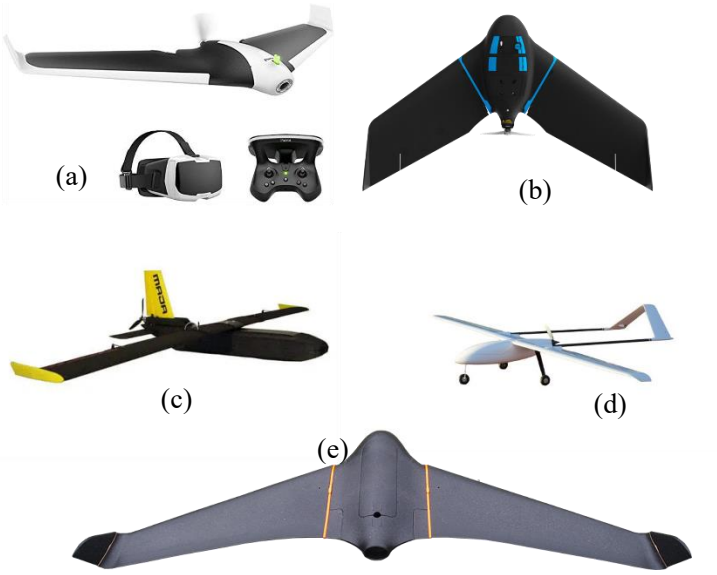

Fig.1- 1Fixed wing drones (a)Parrot disco (b) eBee X (c)Bormatec Maja (d) Albatross UAV (e) Skywalker x8

1.2.2 Flapping wing drone

Flapping wing drones are primarily inspired by insects such as hummingbirds and dragonflies [Design of an active flapping wing mechanism and a micro aerial vehicle using a rotary actuator]. The lightweight and flexible wings are inspired from the feathers of insects and birds which demonstrate the utility of weight and flexibility of wings in aerodynamics. However, these flapping wings are complex because of their complicated aerodynamics. Light, flexible and flapper wings provide the flapper motion with an actuation mechanism. Intensive research on flapping wings has been carrying out by drone community and biologist because of their exclusive maneuverability benefits [An introduction to flapping wing aerodynamics]. Some Flapping wing drones are shown in Figure 1-2. [21-25].

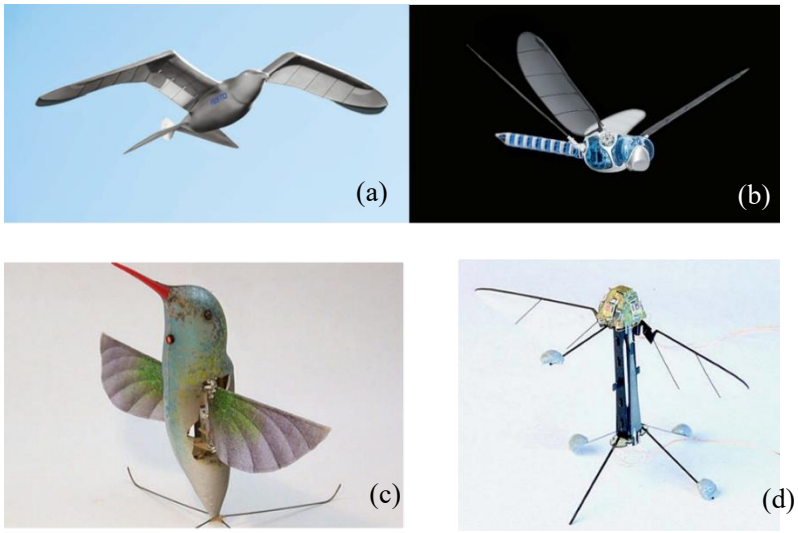

Fig.1- 2 Flapping wing drones (a)Festo SmartBird (b) Festo Bionicopter (c)Nano hummingbird (d) Harvard Microrobotic Fly

1.2.3 Multirotor drone

Main rotor blade produces a forceful thrust, which is used for both lifting and propelling. Multirotor unmanned aerial vehicles are capable of vertical takeoff and Landing (VTOL) and may hover at a place unlike fixed-wing aircraft[26]. Multirotor are designed by number and location of motors and propellers on the frame. For example, the multirotor body can be designed as a traditional helicopter, a tricopter where it has three arms with three motors one on each, or a quadcopter where it has four arms with four motors. Multirotor UAVs can also be configured with a variable number of arms and rotors[27]. Their hovering capability, ability to maintain the speed makes them ideal for surveillance purpose and monitoring. The only concern with Multirotor is that they need more power consumption and makes them endurance limited. Multicopter is divided into specific categories based on number and positioning of motors, each category belongs to a specific type of mission[28], and based on the mission requirement they are classified in various configurations. Some multi-rotor drones are shown in Fig.1-3.

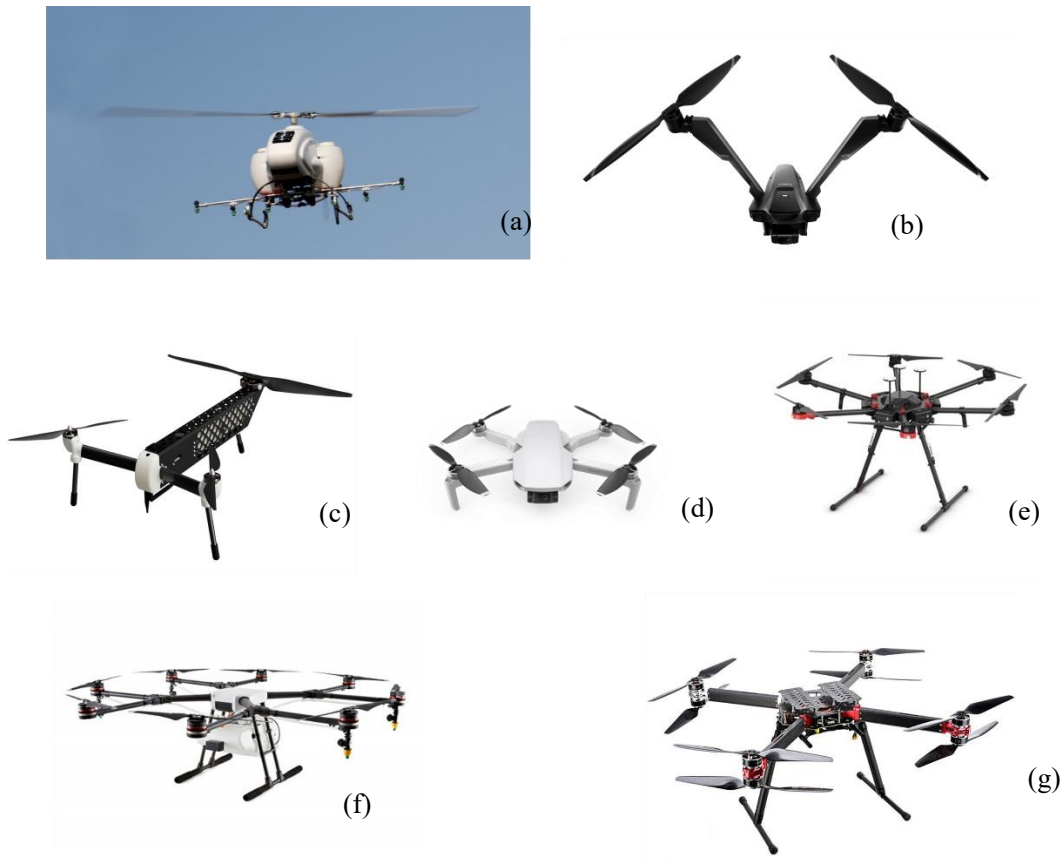

Fig.1- 3 Multirotor drones (a)3WQF170 Helicopter (b) V-Coptr Falcon Bicopter (c) Jupiter Tricopter (d) Mavic Mini Quadcopter (e) Matrice600 hexacopter (f) MG-1 octocopter

1.2.4 Hybrid drone

Most civil UAV applications require that the UAV be able to perform a variety of different and complementary operations in an integrated mission. Some missions require the UAV to take off and land from a limited runway space while flying at a high cruise speed through the area of operation. In addition to this, some tasks require the UAV to fly at a lower cruise speed or be able to hover for stationary measurements. These complementary but different operational capabilities all point to a hybrid UAV concept[29].

1.3 Commercial Multi-rotor Drones

The UAV designs mostly used for commercial applications are fixed-wing and rotary-wing aircraft. Among rotary-wing designs, helicopter and multirotor configurations are the most common. Since multi-rotor UAVs are mechanically simple compared to other types of UAVs and can take off and land vertically, they can fly in smaller spaces and indoors. Therefore, it is very popular in the consumer drone market. Across all applications, multi-rotors represent nearly 90% of the entire market, demonstrating UAV operators have a clear preference for multirotor over fixed wing. For agriculture in particular, nearly one-third of UAV platforms are fixed and two-thirds are multirotor according to the recent research[30]. The following uses “drone” to represent “multirotor drone”. The pioneer of aerial photography drones was the French company Parrot, which launched the AR Drone in 2010.Until then, there were only military drones and no aerial photography drones for general consumers. In addition, the Chinese company DJI has introduced aerial photography drones and industrial drones since 2013, and the phantom series and mavic series drones have become popular products in recent years due to their compact size.The phantom and mavic series drones are compact in size and have become popular in recent years. In addition, the performance of industrial drones such as the inspire and matrice is evolving to meet the demands of various fields, but the size of the aircraft is gradually becoming larger and larger.

1.3.1 Drone size and performance characteristics

Table 1-1and Fig.1-4 show the main drone products on the market in the last 10 years and their sizes, such as Parrot's ARDrone[31], DJI's Phantom series, Mavic series, and professional grade drones such as the Inspire series, Matrice series, and MG series[32].

Table 1- 1 Drone size of recent 10-year products

Year	Product Name	Diagonal Wheelbase [mm]

2010	AR Drone	360
2012	Flame Wheel F330	330
2012	Flame Wheel F550	550
2012	S800	800
2013	Phantom	350
2013	Phantom2 Vision	350
2013	Phantom2	350
2014	S1000	1000
2014	Phantom 2 Vision+	350
2014	S900	900
2015	Inspire1	581
2015	Phantom3 (Professional&Advacned)	350
2015	Matrice 100	650
2015	Phantom3 Standard	350
2016	Agras MG-1	1520
2016	Phantom3 4K	350
2016	Phantom 4	350
2016	Matrice 600	1133
2016	Mavic Pro	335
2016	Matrice 600 Pro	1133
2016	Inspire 2	605
2017	Phantom4 Pro	350
2017	Spark	170
2017	Matrice 200 Series	643
2017	Agrass MG-1S & MG-1P	1500
2018	Phantom4 Advanced	350
2018	Mavic Air	213
2018	Mavic 2 Pro	354
2019	Phantom4 RTK	350
2020	Mavic Mini	213
2020	Mavic Air 2	302
2020	Matrice 300 RTK	895
2020	Mavic Mini 2	213

2021	Mavic Air 2S	380
2021	Mavic Mavic 3	302

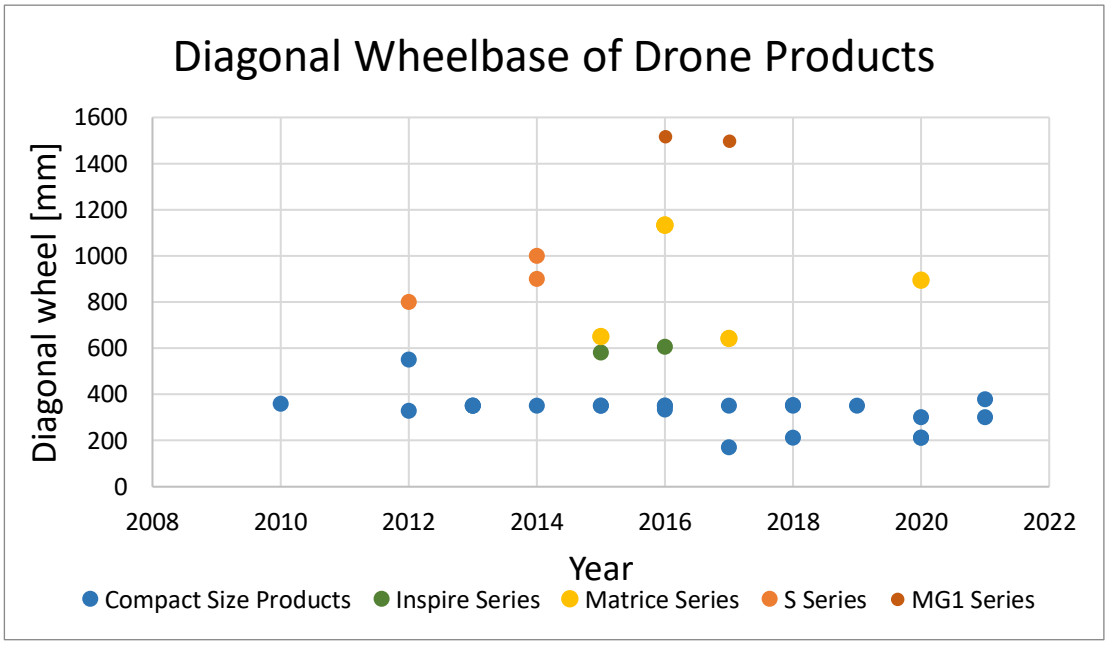

Fig.1- 4 Diagonal Wheelbase of Drone Products

As shown in Fig.1-4, smaller drones are being developed to meet the needs of the general users. The DJI Phantom series and Mavic series drones are compact in size and have become popular products in recent years. On the other hand, the performance of industrial drones such as the DJI Inspire series and Matrice series drones are evolving to meet the demands of various fields, but the size of the aircraft is getting larger.
The small size of the drone makes it easy to transport. Compared to larger size drone, the risk of collision is lower, making them easier to operate. However, the propellers of small drones are small, and they do not have much payload, their scalability is low, which is a disadvantage of small drone. When using a large drone, it is more difficult to transport, and its large size means that you need to constantly check for obstacles in your surroundings. However, since the propeller is large, the payload is better, and it is highly scalable, allowing for better-performing cameras and other external sensors to be installed. Table 1-2 summarized the features of small drone and large drone.

Table 1- 2 Features of small drones and large drones

	Small drone	**Large drone**
Carry and delivery	Easy	Difficult
Operation	Easy	Difficult
Risk	Low	High
Load capacity	High	Low
Sensors	Small camera	Professional camera, external sensors

1.4 Purpose

While compact drones are popular with consumers, and more large size industrial drones are being developed to meet the needs of various industries. The development of a compact drone that incorporates the advantages of both large and small drones is expected.

The aim of this research is to improve the structure of conventional multi-rotor drone and create a drone that has the advantages of both small and large drone.

In chapter 2, we propose a drone structure to miniaturize the multi-rotor drone without changing the rotors and propellers. The proposed structure reduces the size by shortening the distance between the motors and by making a height difference between the rotors.

The reduction in rotor distance leads to a reduction in rotational inertia, causing it more difficult to control. The disturbance caused by downwash in the overlapping region will also affect the control performance [33] and the downwash is difficult to model. In chapter3, an efficient active disturbance rejection controller is proposed for the proposed structure.

In Chapter 4, the proposed controller is compared and evaluated on different drones.

Chapter2

Overlapping Rotor Design for Miniaturization of Multi-Rotor Drones

There are many applications where drones can be used as an efficient alternative to manual labor[34]. As mentioned in the previous section, the development of a compact drone that incorporates the advantages of both large and small drones is expected.
On the other hand, the use of drones comes with risks[35] and often the use of propeller guards [36] provides protection, but the exposure of the propeller over the fuselage is still dangerous. A spherical guard to cover the fuselage has also been proposed[37], which would make the fuselage even larger, contrary to our aim of miniaturization.
In this chapter, a multi-rotor drone structure is proposed to miniaturize the drone size without changing the rotors and propellers.

2.1 Overview of Compact Drone Structure

In this chapter, a compact drone structure is proposed. In proposed structure, the rotors are overlapped by setting a height difference between adjacent rotor blades to realize a compact size.

2.1.1 4-rotor drone using proposed compact structure

Fig.2-1 shows the rotor layout of a conventional quad-rotor drone and the proposed drone. The left figure in Fig.2-1 shows the layout and area of the rotor blades of the conventional quad-rotor drone. The middle figure in Fig.2-1 shows the layout and area of the rotor blades of the proposed drone structure that overlaps the rotation area by setting a height difference between adjacent rotor blades. The right figure in Fig.2-1 shows a side view of the rotor blades of the proposed structure.

Defining the radius of the rotor blade as L and the minimum size polygon enclosing the rotor blade as the aircraft size, the minimum size (rectangle size) of the conventional drone is 16.00 L^2 and the size (rectangle size) of the proposed drone is 11.66 L^2. In means that the aircraft size can be reduced by 27.14% by using the proposed structure compared to the conventional structure.

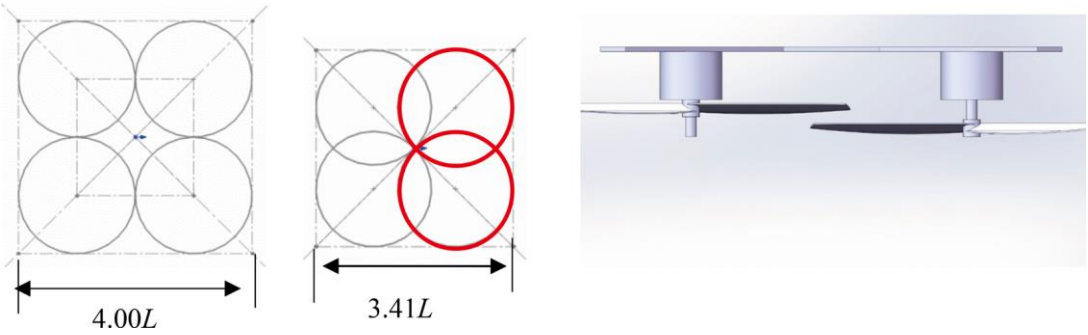

Fig.2- 1 Rotor layout of conventional quad-rotor drone (left) Rotor layout of proposed quad-rotor drone (center) Side view of proposed drone structure (right)

The compact structure with a height difference can also save more area as shown in Fig. 2-2, but the structure is expected to be complicated and difficult to manufacture because of the need to set the height of each propeller is different. The reduction in rotor distance will cause it to be more difficult to control. On the other hand, the diagonal rotors of proposed structure are on the same level that makes implementation much simpler.

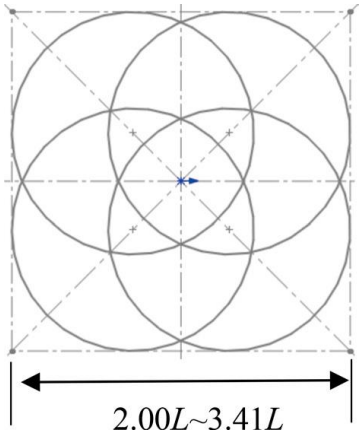

Fig.2- 2 Compact structure with four-height rotor layout

2.1.2 6-rotor drone using proposed compact structure

The proposed structure is applicable not only to 4-rotor drones but also to 6-rotor and 8-rotor drones. Conceptual drawings of various proposed drones are shown in figure 2-3.

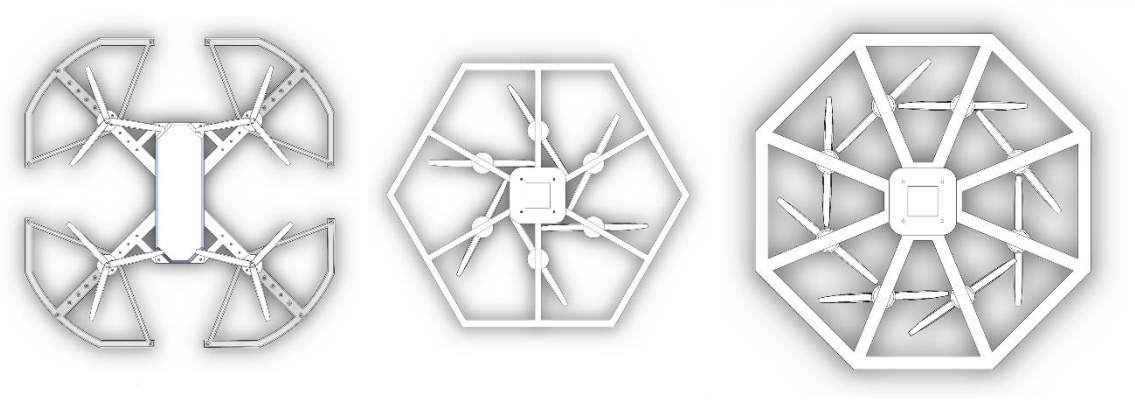

Fig.2- 3 Conceptual drawings of proposed 4-rotor, 6-rotor and 8-rotor drones

The left figure in Fig. 2-4 shows the rotor layout of conventional 6-rotor drones and the minimum size (hexagon size).

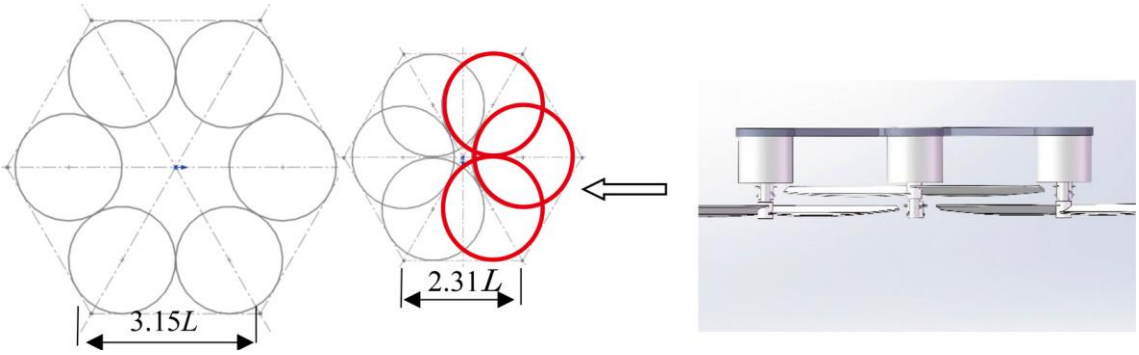

Fig.2- 4 Rotor layout of conventional 6-rotor drone (left) Rotor layout of proposed 6-rotor drone (center) Side view of proposed drone structure (right)

The middle figure in Fig. 2-4 shows the compact rotor layout and size (hexagonal size) using proposed structure. The rotating area per rotor blade is the same for the conventional drone and the proposed drone. However, the size of the proposed drone is 53.6% (13.86 L^2) smaller than that of the conventional drone (25.86 L^2). The right figure in Fig. 2-4 shows the side view of the rotor blade of proposed drone. There is a height difference between the adjacent rotor blades, and the rotor blades that are two rotor blades away from each other are set at the same height.

2.1.3 8-rotor drone using proposed compact structure

Next, we introduce the 8-rotor drone using the proposed structure.

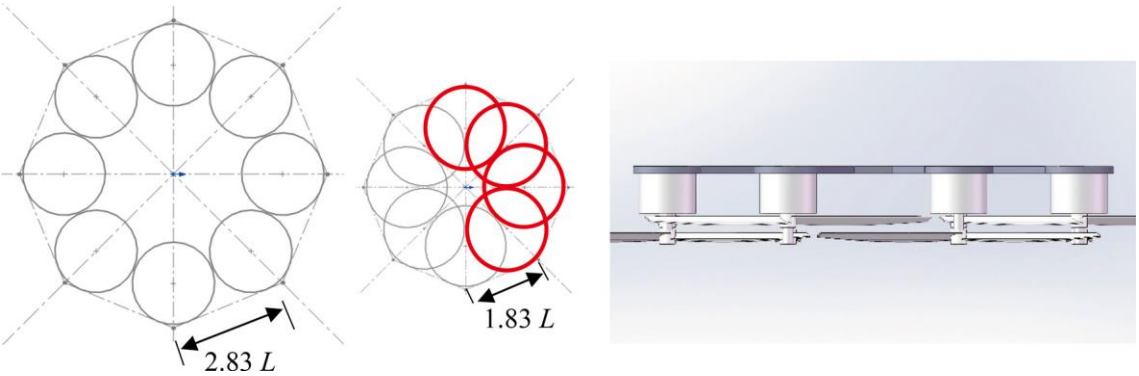

Fig.2- 5 Rotor layout of conventional 8-rotor drone (left) Rotor layout of proposed 8-rotor drone (center) Side view of proposed drone structure (right)

The left figure in Fig.2-5 shows the rotor layout of a conventional 8-rotor drone and the minimum size (octagon size). The middle figure in Fig. 2-5 shows the rotor layout and size (octagon size) using the proposed structure. The size of the proposed drone is 45.66% (17.68 L^2) smaller than that of the conventional drone (38.72 L^2 if L is the radius of the rotor blade). The right figure in Fig.2-5 shows the side view of rotor blades of the proposed drone structure.

Fig.2-6 shows a graph comparing the size of the conventional and proposed structure for the 4 to 8-rotor drones.

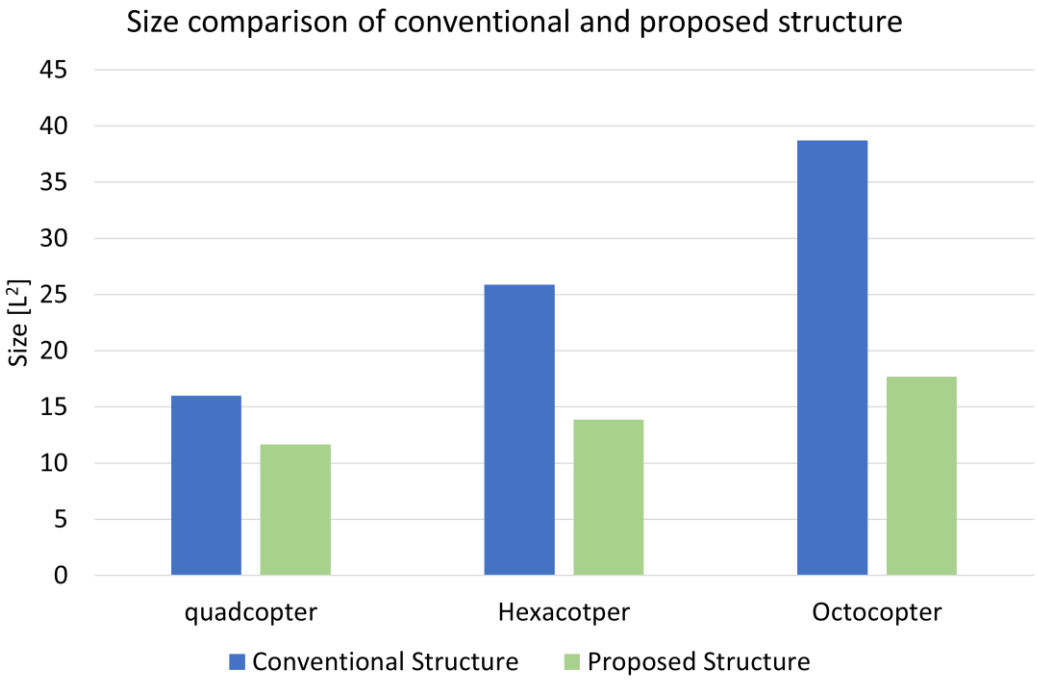

Fig.2- 6 Size comparison of conventional and proposed structure

Compared to the drone with the conventional structure, the proposed structure can reduce the increase of the aircraft size even when the number of rotors increases.

In particular, the size of the 6 and 8-rotor drones with the proposed structure is almost the same as that of the conventional 4-rotor drones. The small size of the aircraft can reduce the risk of colliding with other objects. In a limited operational environment, the proposed structure can achieve the performance of an 8-rotor drone with the size of a

conventional 4-rotor drone. In general, the number of rotors of a drone corresponds to the upper limit of its payload [38] and the larger the number of rotors, the larger the upper limit of payload [39].

2.1.2 Bottom mounting of the motor

In most conventional drones, the rotor blades are placed at the top of the fuselage frame. If this design is directly applied to the proposed structure with overlapping rotor blades, the rotor area covers the sensors in flight controller including the pressure sensor, it will be affected by the downwash generated by the rotor blade. In this study, we propose an airframe structure in which the rotor blades are placed under the fuselage as shown in Fig.2-7 to improve this problem. We have confirmed through experiments that this structure can reduce the influence on the sensor.

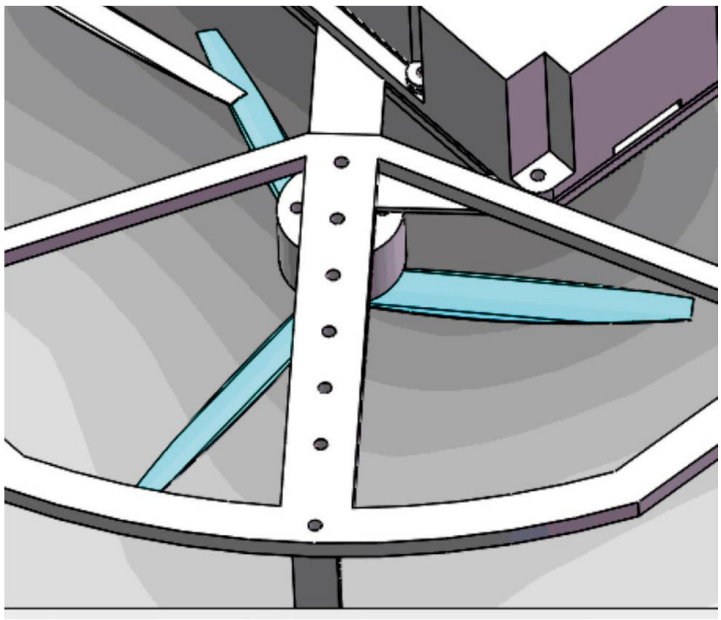

Fig.2- 7 Bottom mounting of rotors

As shown in Fig. 2-8, when a drone flies, the upper surface of the drone moves forward, so it is likely to collide from the upper surface. Therefore, by placing the rotor blades on the lower surface, the risk of collision can be reduced. The large exposed area at the top of the rotor blade, which has been a problem in conventional drone safety measures, can be

eliminated. The safety, size, and weight of the proposed structure and the conventional structure with safety measures are compared as shown in Table 2-1. The weight of the proposed structure is the lightest among the models compared due to its compactness.

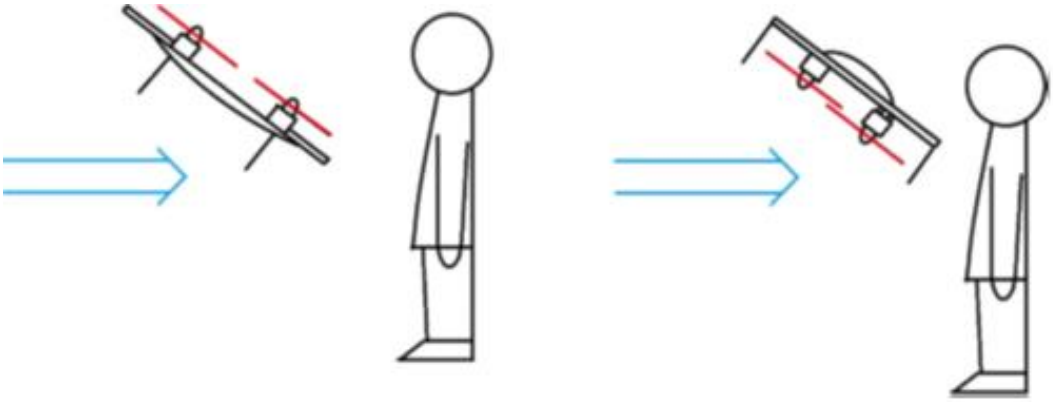

Fig.2- 8 Image in case of collision

When a drone flies, the upper surface of the drone moves toward the front, so it is likely to collide from the upper surface, and the bottom mounting of rotor blades can reduce the risk in the event of a collision.

Table 2- 1 Comparison of proposed drone and conventional drone safety measures

	Size	Weight	Safety
Proposed Structure	I	I	II
Conventional Drone with Propeller Guard	II	II	III
Conventional Drone with Sphere Guard	III	III	I

A comparison of the proposed drone and a conventional drone is made from three perspectives: size, weight, and safety of the drone. The proposed drone is compared with a conventional drone in terms of size, weight, and safety. The size is I to III in order of decreasing, the weight is I to III in order of decreasing and the safety is I to III in order of increasing.

2.2 Control algorithm

In general, the control of a drone can be divided into two parts: the first is the inner loop that perform attitude control, and the second is the outer loop that controls the position of the drone from a global perspective by means of external operation signals from a radio station or ground station. The inner loop control is shown in upper block diagram of Fig.2-9, and the outer loop control is shown in bottom block diagram of Fig.2-9. In conventional drone control, acceleration signals are not used for position and velocity control in the IMU (inertial measurement unit), which measures acceleration and angular velocity in each of the three axes, but are only used to estimate the attitude angle, angular velocity, position and velocity.

In this researcj, we use cascade controller for attitude and position control[40]. To achieve the goal of increasing the response speed and improving the robustness to external disturbances, the acceleration feedback structure shown in Fig.2-9 is used. The difference from the conventional inner loop is the acceleration control part highlighted in Fig. 2-9. The inputs to the outer loop are the set values of latitude (X_ref) and longitude (Y_ref), and the inputs to the inner loop are the set values of attitude (Pitch_ref, Roll_ref, Yaw_ref) calculated from the acceleration error.

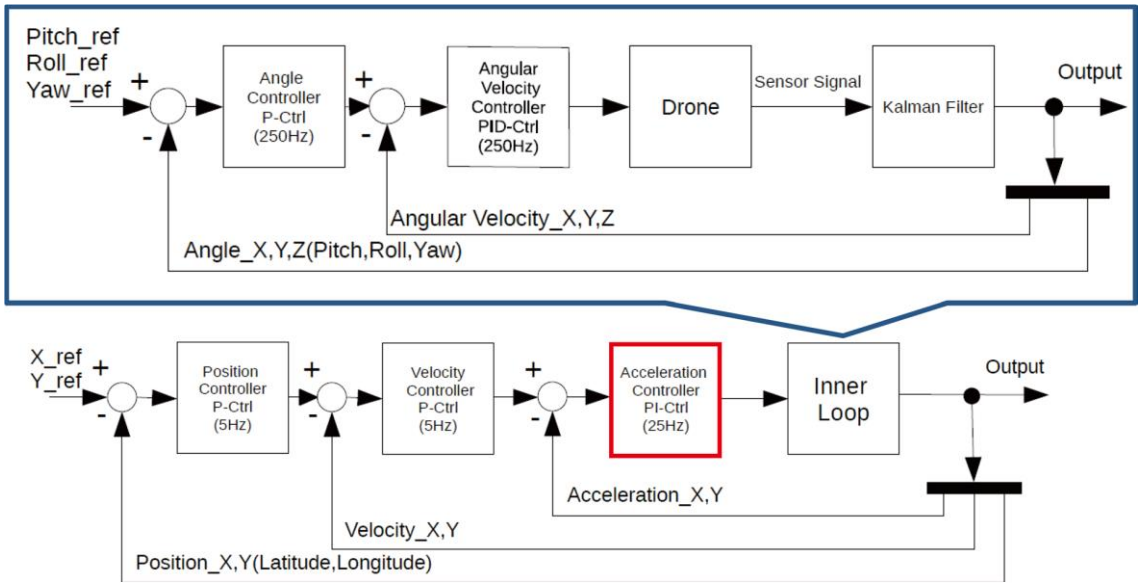

Fig.2- 9 Block diagram of horizontal position control

2.3 Control performance evaluation and efficiency comparative experiment

2.3.1 Implementation of 4-rotor drone with proposed structure

Fig.2-10 shows the appearance (front, top, side, and diagonal) of the proposed drone (the proposed quad-rotor structure). The drone is equipped with three CPUs (CPU1, CPU2: STM32F103, CPU3: Raspberry PI Zero W), each of which controls the attitude, gimbal, and camera. Fig.2-11 shows the relationship between the CPUs and control targets. The hardware is integrated into a frame board as shown in Fig. 2-12. The case and guard of the fuselage are made of nylon material and processed by a 3D printer. The distance between diagonal motors is 180 [mm], the overall size is 350 [mm] × 350 [mm] × 129 [mm], and the weight is 460 [g]. 6 [inch] propellers and EMAX 2306 motors are used. The specifications of the implemented drones are shown in Table 2-2.

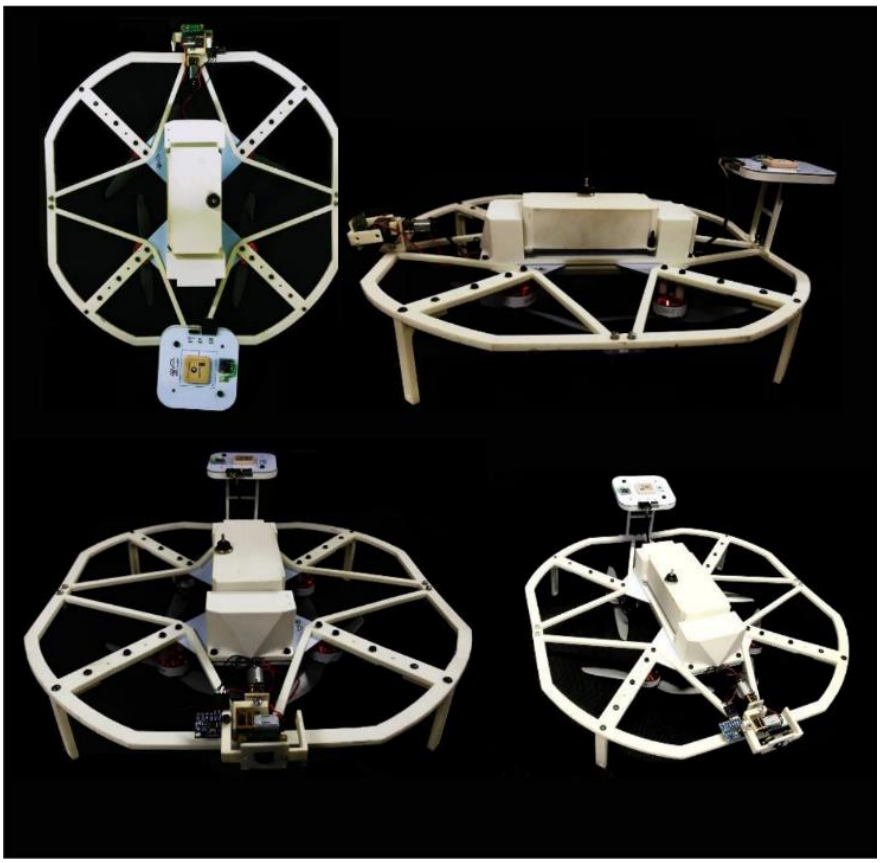

Fig.2- 10 Implementation of a 4-rotor drone with the proposed structure

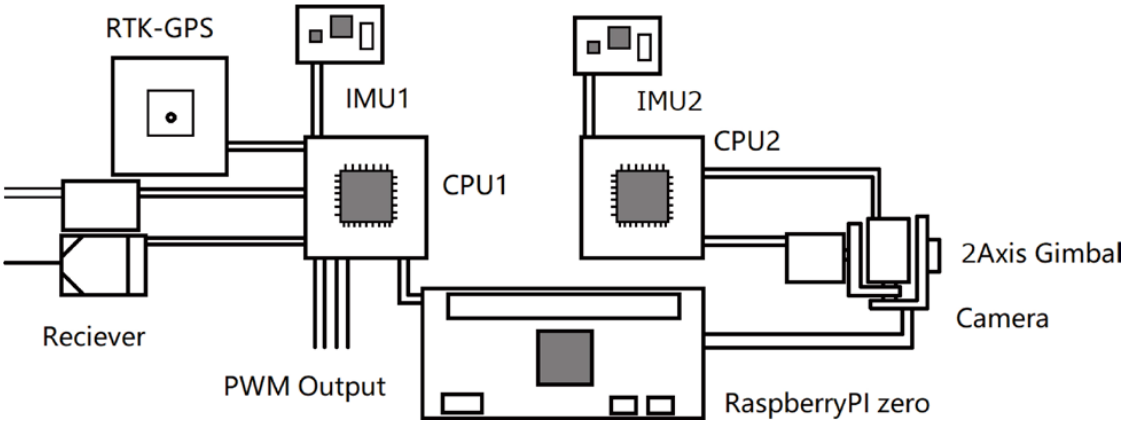

Fig.2- 11 Relationship between CPU and each control target

The flight controller and gimbal controller use a 72 [MHz] microcontroller. The RaspberryPI ZERO is used to collect, process, and transmit the images captured by the camera mounted on the aircraft.

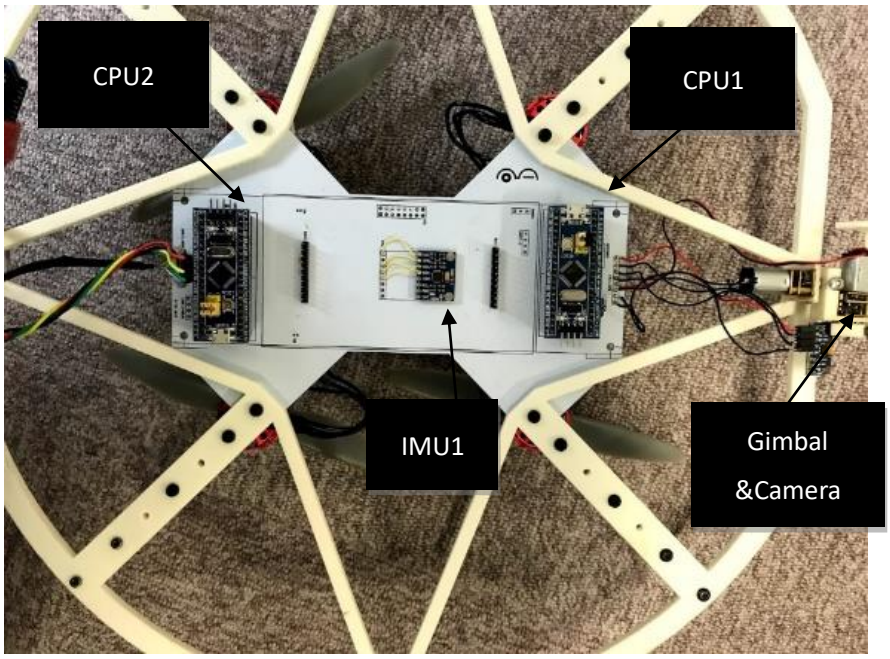

Fig.2- 12 Frame circuit board

Table 2- 2 Specifications of the implemented proposed drone

Dimensions	350 [mm]×350 [mm]×129 [mm]
IMU sensor	MPU6050, HMC5883L
Motors	EMAX RS2306 2400KV
Maximum flight speed	2.5 [m/s]
Maximum tilt angle	15°
Gimbal controllable range	Pitch: 0-15°
Camera sensor	IMX219
GPS Module	Ublox M8P

2.3.2 Control performance evaluation experiment

We compared the control performance of the conventional structure drone and proposed structure drone. The conventional structure and proposed structure are realized by adjusting the rotor distance of implemented drone that shown in Fig. 2-10. The same attitude controller was used for comparison. The experiment was conducted in an indoor environment, and the flight altitude was set to 1.5 [m]. The pitch and roll

angles were measured and collected by telemetry in real time. Fig.2-13 and Fig.2-14 show a comparison between the conventional and proposed structure. Figures 12 and 13 show the results of the conventional and proposed drone structures. In each figure, the red line represents the control command, and the blue line represents the actual control result.

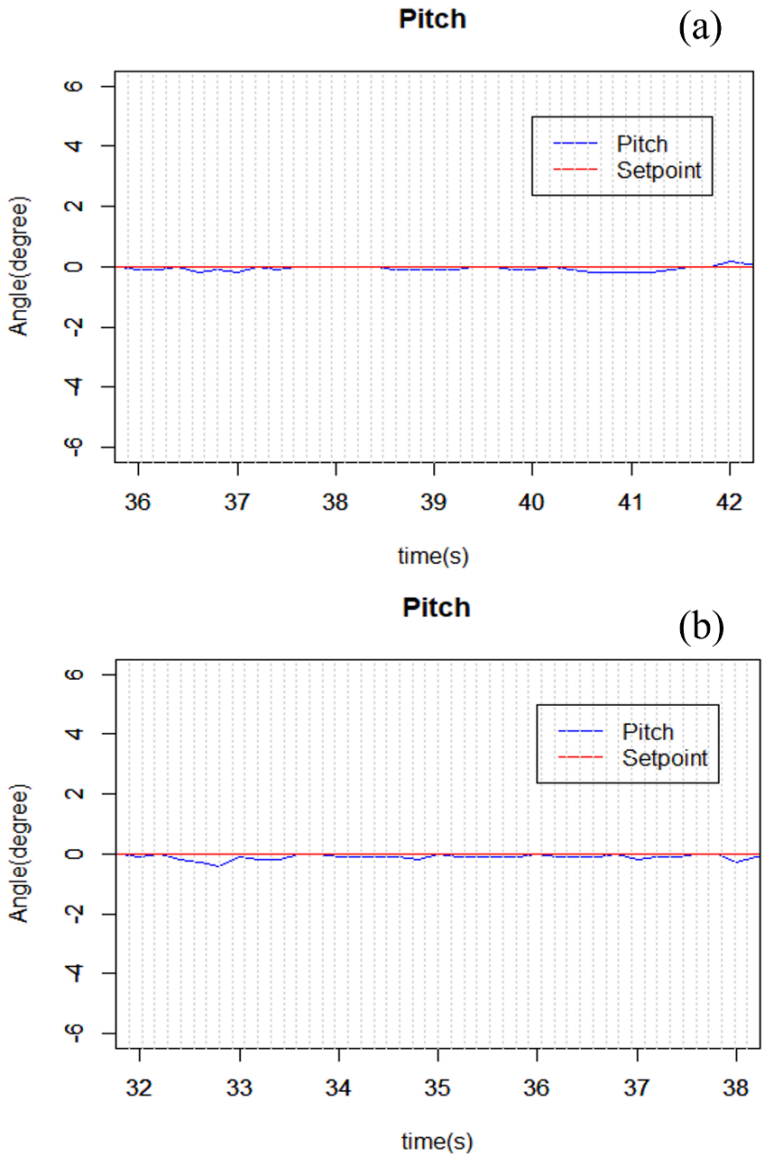

Fig.2- 13 0-degree response of conventional and proposed structure

Table 2- 3 2-3 IAE comparison

Method	IAE
Conventional drone structure	0.56
Proposed drone structure	0.78

The hovering curve (Fig.2-13) shows that the maximum deviation of the conventional structure is 0.4° and that of the proposed structure is 0.8°. Table2-3 shows the hovering IAE (Integral Absolute Error) of each structure. Though both structures can remain stable with same controller, the proposed structure showed a larger IAE. The reduction in rotational inertia, and the disturbance caused by downwash in the overlapping region may affect the control performance.

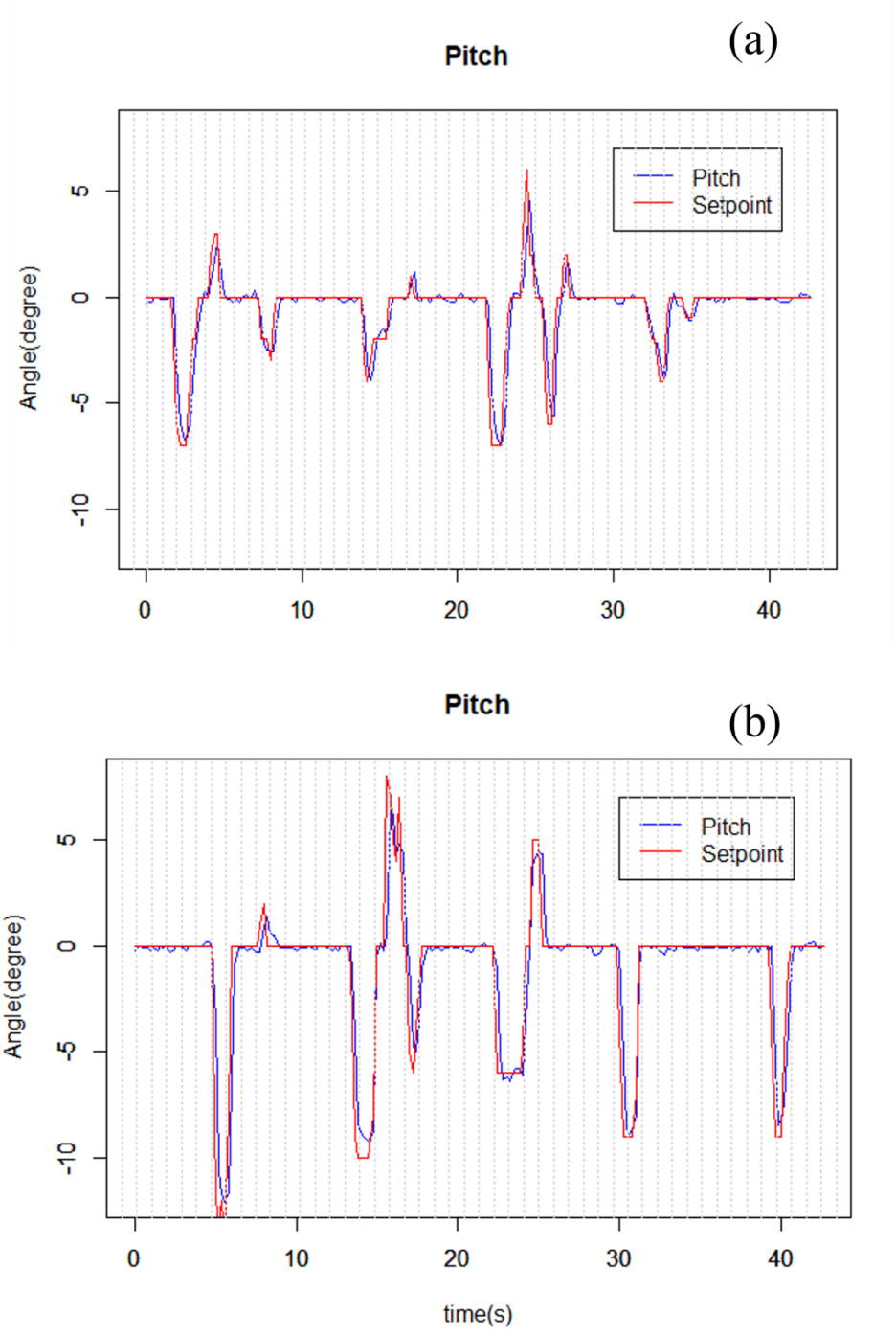

Fig.2- 14 Response test of conventional and proposed structure

2.3.3 Efficiency comparative experiment

In this section, based on measurement experiments and theoretical

considerations, we show that the proposed drone can output sufficient thrust and has superior propulsive efficiency to conventional drones when compared with drones of similar size.

For this purpose, we first conducted experiments to measure the thrust and propulsive efficiency of the proposed drone and the conventional drone using the same propeller. Through the experiments, we confirm that the proposed drone can generate sufficient thrust. We also determine how much the propulsive efficiency of the proposed drone decreases compared to that of the conventional drone. Next, we compare the thrust efficiency of conventional drones with propellers of different diameters using a mathematical formula. This allows us to determine how much the propulsive efficiency of the conventional drone with propellers of the same diameter as the proposed drone decreases compared to the conventional drone with propellers of the same diameter as the proposed drone.Finally, we compare the propulsive efficiency of the proposed drone and the conventional drone of the same size by combining the results of the experiment and the mathematical comparison. As a result, we show that the proposed drone is superior to the conventional drone in terms of propulsive efficiency.

First, we describe an experiment to measure the thrust and propulsive efficiency of the proposed drone and a conventional drone using the same propeller. In this measurement experiment, we confirm whether the proposed drone can output sufficient thrust (thrust that can secure the weight in flight and the payload for carrying the camera (460 [g] in total)) and compare the propulsive efficiency of the proposed drone with that of a conventional drone. There are various methods of measuring the thrust of a propulsion mechanism that consists of only a motor and a propeller. The framework of this experiment was constructed based on one such reference [41]. This experiment is conducted in the environment shown in Fig.2-15.

Fig.2- 15 Efficiency comparative experiment environment

The drone is placed on top of the digital weight scale in the opposite direction, and the aircraft is powered by a stabilized power supply. The voltage is fixed at 12 [V], and we measure the change in thrust as the current is varied. The thrust force is defined as the numerical value of the digital gravimeter, and the efficiency is defined as the thrust force divided by the product of the voltage and current. The results of the measurement experiment are shown in Fig.2-16. Fig.2-16-a shows the result of thrust measurement experiment. Fig.2-16-b shows the result of efficiency measurement experiment.

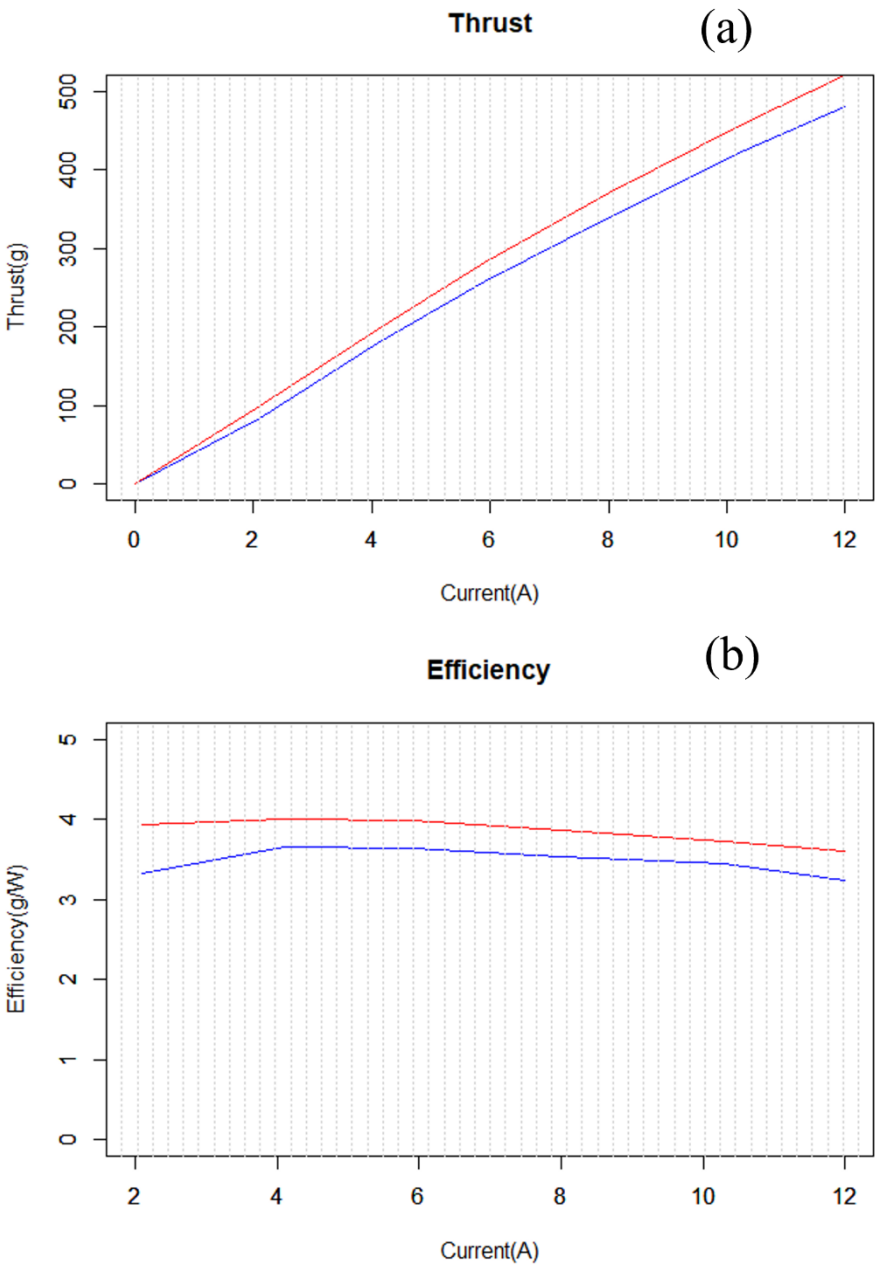

Fig.2- 16 Result of thrust and efficiency comparative experiment

The blue line in the figure shows the result of the proposed drone and the red line shows the result of the conventional drone. From the experimental results, it can be confirmed that the proposed drone can output sufficient thrust. Furthermore, the operating current and propulsive efficiency of the proposed drone are 11.4 [A] and 3.37 [g/W],

while the operating current and propulsive efficiency of the conventional drone are 10.3 [A] and 3.72 [g/W] when hovering is assumed. In other words, the propulsive efficiency and thrust of the proposed drone are about 90.5% of those of the conventional drone.

Next, we describe a comparison of the thrust efficiency of conventional drones with propellers of different diameters using mathematical equations under the same assumptions as in the experiment. In the experiment, measurements were made assuming hovering, so we use static thrust as the thrust for comparison. Suppose that we have two propellers with different diameters, propellers i and i = {1, 2}, respectively. The static thrust T_i [kg], torque Q_i[kg · m], and power output W_i [W] of propeller i are

$$T_i = C_{T,i}\rho n_i^2 L_i^4, Q_i = C_{Q,i}\rho n_i^2 L_i^5, W_i = Q_i 2\pi n_i, \quad (2\text{-}1)$$

[42].

$C_{T,i}, C_{Q,i}, n_i, L_i, \rho$ are the thrust coefficient, torque coefficient, rotation speed [1⁄s], and diameter [m] of propeller i, respectively. We also assume that propeller 2 is smaller than propeller 1 and that the following holds between their diameters: $L_2 = \alpha L_1, \ \alpha \leq 1$. Furthermore, propellers 1 and 2 differ only in their diameters and have identical characteristics. In other words, assume that $C_{T,1} = C_{T,2} = C_T, C_{Q,1} = C_{Q,2} = C_Q$. To facilitate the comparison of propulsive efficiency, the output of each propeller is assumed to be non-zero and constant. In other words, we assume that $W_1 = W_2 = W \neq 0$. Under this assumption, the comparison of the propulsive efficiency T_i / W_i is equivalent to the comparison of the thrust T_i. Therefore, the comparison of thrust will be used as the comparison of propulsive efficiency. Under the above assumptions, the static thrust T_2 due to propeller 2 is equal to the static thrust T_1 due to propeller 1

$$T_2 = \left(\sqrt[3]{\alpha}\right)^2 T_1 = \beta T_1, \quad (2\text{-}2)$$

If we set propeller 2 so that the conventional drone composed of propeller 2 has the same size as the proposed drone, we can see from

Eq.2-2 that L_1 =2L and L_2 ≈1.705L, or α≈0.85. At this time, the propulsive efficiency and thrust of the conventional drone configured with propeller 2 is approximately 89.7% of that of the conventional drone configured with propeller 1. In actual implementation, the diameter of the propeller can only be changed every 1 [inch], considering that off-the-shelf propellers are used. Comparing the propulsive efficiency with $\alpha \leq 0.85$ so that the conventional drone composed of propeller 2 is the same size as the proposed drone composed of propeller 1, the thrust of the conventional drone composed of propeller 2 is smaller than that of the conventional drone composed of propeller 1. For example, β ≈ 0.826 when L_1 = 4 and L_2 = 3 [inch], and β ≈ 0.862 when L_1 = 5 and L_2 = 4 [inch]. In addition, for the case of L_1=7 [inch], when L_2 =6 [inch], α>0.85, so L_2 =5 [inch] is considered appropriate for comparison, and the β for that case is β≈0.80.

Finally, we discuss the propulsive efficiency of the proposed drone and the conventional drone based on the results of the experiment and the comparison by formula. First, the experimental results show that the propulsive efficiency of the proposed drone is about 90.5% of that of a conventional drone using a propeller of the same diameter. On the other hand, the propulsive efficiency of the conventional drone with the same size as the proposed drone by changing the propeller diameter was about 89.7% of that of the conventional drone with the same diameter propeller. Comparing these results, the propulsive efficiency of the proposed drone is superior to that of the conventional drone when compared with a drone of the same size. In addition, the advantage of the proposed drone is higher in actual implementation because the choice of propeller diameter is limited. Furthermore, the thrust of the proposed drone can be increased by increasing the number of rotors due to its compactness. Therefore, the energy loss caused by the proposed structure is not considered to be a significant problem.

2.4 Cooperative flight experiment of the proposed

drone swarm

In this section, we construct cooperative flight control of multiple proposed drones and suggest a framework for high-precision measurement by drones through demonstration experiments in outdoor environments. Conventional drones, especially those equipped with propeller guards, are large in size, and as a result, it is difficult for each drone to perform measurements at a close distance from each other. On the other hand, the size of the proposed structure is smaller than that of conventional drones, even when the number of rotors is increased, so that the drones can easily measure each other at close range. In addition, the proposed structure, which is designed to be safe, makes it difficult for a collision between drones to lead directly to a drone crash. Therefore, the proposed drone is suitable for cooperative flight by multiple drones. 3 of the proposed drones were fabricated (Fig.2-17), and their cooperative flight experiments were conducted in an actual breeding field. The target field is a data farm located in Sarabetsu, Hokkaido, as shown in Fig.2-18, and the experiment was conducted on August 16, 2017.

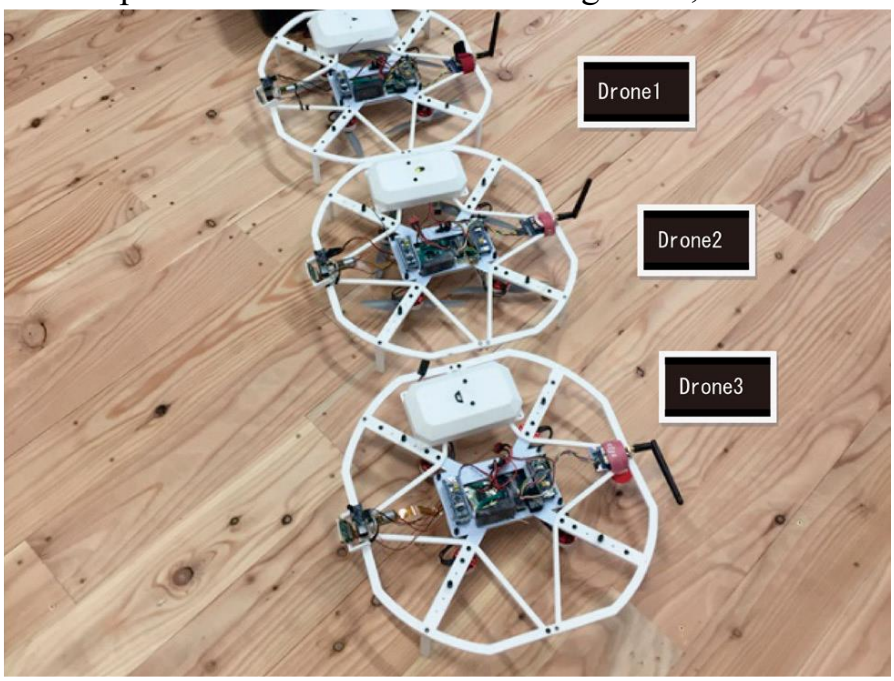

Fig.2- 17 Implemented drones in cooperative flight experiment

Fig.2- 18 The data farm

The cooperative flight of the 3 drones is performed by connecting the ground station to each aircraft via wireless XBee modules, as shown in Fig.2-19. The data packet exchanged between each drone is as follows: <time 1, destination location information 1, camera operation 1>. The data is shared at a frequency of 5 [Hz]. Destination position information (longitude, latitude, altitude) is calculated at the ground station and sent to each drone along with the camera operation (tilt of the gimbal and shooting command). Each drone moves to its own location and takes pictures according to the received packets. In the cooperative flight experiment, we execute a plan in which three drones fly to their respective target points in the same direction and at the same speed.

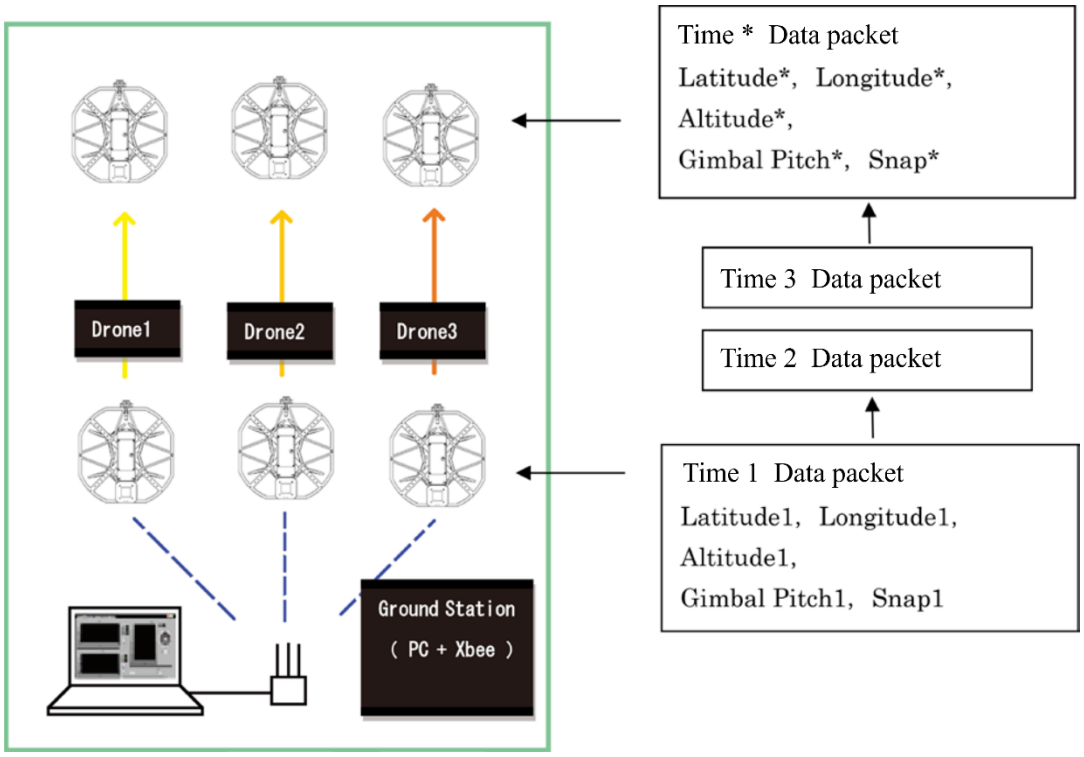

Fig.2- 19 Diagram of communication

As shown in Fig.2-20, a cooperative flight by three drones was realized, and a sample image captured by a drone is shown in Fig.2-21. The cooperative flight framework enables us to capture images of the crop from multiple viewpoints simultaneously. This is expected to improve the accuracy of 3D reconstruction by suppressing the influence of factors such as wind, which can deteriorate the accuracy of 3D reconstruction.

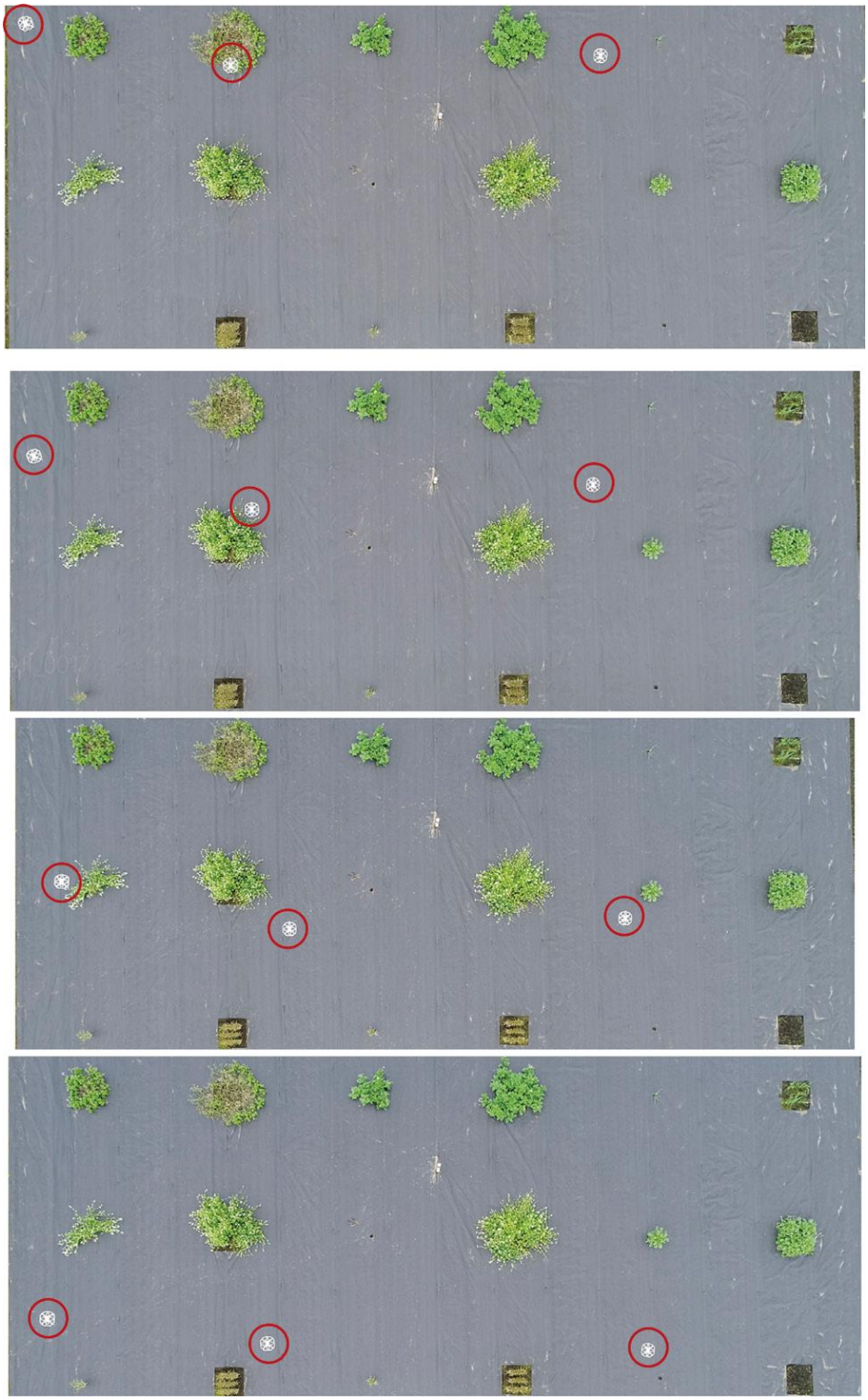

Fig.2- 20 Cooperative flight experiment

Fig.2- 21 A sample image captured by a drone

2.5 Conclusion

A multi-rotor drone structure is proposed which has higher safety than the conventional propeller guard and can make the size compact by making rotor blades overlapped, and by setting a difference in height on adjacent rotor blades. It is shown that the proposed 4-rotor drone (quadcopter), 6-rotor drone (hexacopter) and 8-rotor drone (octocopter) can achieve about 27%, 46% and 54% size reduction respectively compared with conventional structure. In order to evaluate the proposed method, a quad-rotor drone with proposed structure is implemented, the propulsion capability and control performance comparison experiment is performed in an indoor environment. In addition, we made multiple proposed drones, and demonstration are conducted in an outdoor environment, suggesting a framework for remote sensing using drones.

Chapter3

Efficient Active Disturbance Rejection Control using a Reduced-order Observer

The compact drone structure is presented in chapter 2, and the attitude control performance is compared using conventional cascade PID controller. A model free and anti-disturbance controller is expected due to the disturbance caused by overlapping propellers is difficult to model, and the disturbance caused by the overlapping propellers also affect the control performance. In this chapter, by combining the conventional cascade control with reduced order LADRC, an efficient attitude controller is proposed

3.1 Drone Attitude Controller

Attitude control is the most essential part of a multi-rotor drone because the velocity and position controls are achieved by controlling the attitude. A stable attitude control improves the performance of the velocity and position controls. The cascade control method is widely used in flight controllers compared with the single closed-loop attitude control method since it achieves setpoint tracking with less overshoot and faster response [43][44].

Han proposed the active disturbance rejection control (ADRC) method [45][46] that estimates and removes disturbances using an extended state observer. By rejecting the estimated disturbance, the system model approximately transforms into an integral chain. Gao proposed a linearized ADRC (LADRC) method using a PD controller and a linear ESO (LESO) [47], simplifying the conventional ADRC method. Also, the ADRC method has been developed for attitude control in drones [47-53].

Due to the use of inertial sensors, drones have high precision. The

observation of the feedback signal in a conventional ADRC algorithm can be further omitted, and the disturbance rejection can be achieved by directly estimating the total disturbance value. This is a more simplified implementation of the ADRC method on a flight controller. Due to the robustness and responsiveness of the cascade closed-loop structure, we proposed a cascade-LADRC attitude controller in which a first order LESO is used to simplify the conventional LADRC algorithm for disturbance estimation. Through simulation, the control performance of the proposed method was compared and evaluated in relation to conventional control methods.

3.1.1 Cascade PID attitude controller

With the improvement in the performance of inertial sensors, drone attitude estimations and angular velocity measurements have become more accurate and reliable. Using the data of these sensors for feedback makes drone control easier and more stable. Usually, a drone uses a 3-axis gyroscope to measure the body's angular velocity and then uses a 3-axis accelerometer to estimate the body's attitude. The conventional control methods that use this data for attitude control are described below.

Compared with a single closed-loop attitude control method (Fig.3-1), the widely used angular velocity cascade PID controller has a faster response speed and a smaller overshoot.

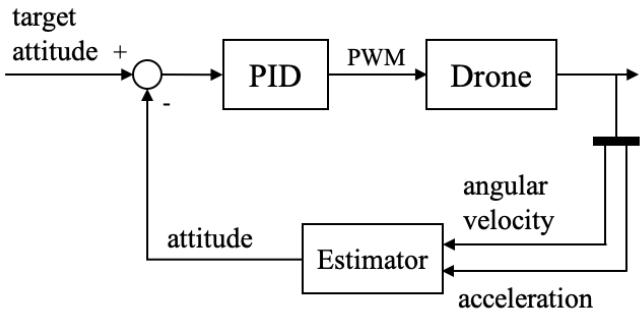

Fig.3- 1 Block diagram of a single closed-loop PID controller

A cascade controller for an attitude control block diagram is shown in Fig.3-2. The angle error is taken as the input of the attitude controller (P controller) to calculate the angular velocity setpoint, and then the angular velocity controller (PID controller) calculates the PWM output for the

motors. The structure is simple, and the parameters are few, so it is easy to implement the algorithm with a microcomputer as a flight controller.

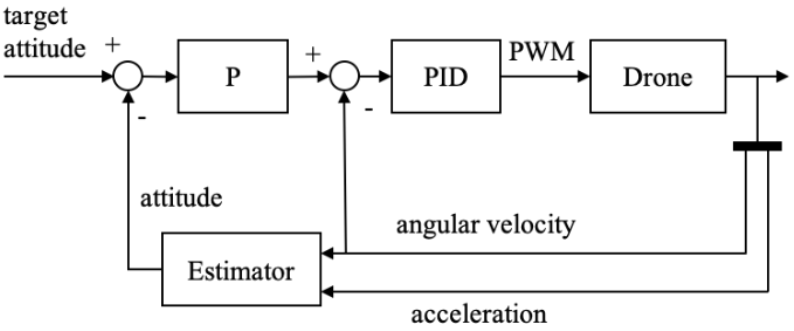

Fig.3- 2 Cascade control block diagram

3.2 Linear active disturbance-rejection control

3.2.1 Linear active disturbance-rejection control

Conventional nonlinear ADRC applies ESO to estimate system disturbance and achieve robustness through real-time disturbance rejection. It is characterized by complex structural implementation and has many parameters [54]. LADRC linearizes the ESO, and the parameters are related to the bandwidth of the observer. Furthermore, the control model is simplified using a simple PD controller. The block diagram of the LADRC is shown in Fig.3-3.

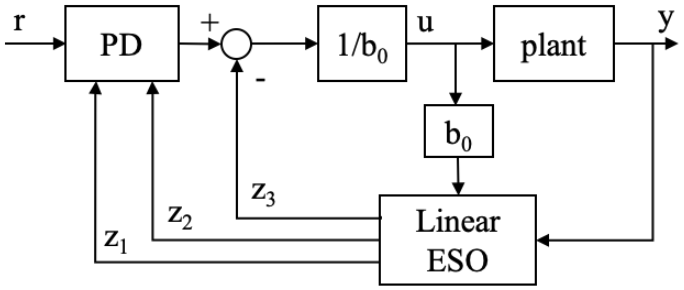

Fig.3- 3 LADRC block diagram with full-order LESO

When only considering the angular acceleration and torque of a drone in one dimension, the attitude control model with the torque input and angle

output can be regarded as a second-order system. For a second-order system,

$$\ddot{y} = -a_1\dot{y} - a_2 y + w + bu, \tag{3-1}$$

where y and u denote the system's output and input, respectively, a_1 and a_2 denote the system dynamic coefficients, respectively, and w is the external unknown disturbance. b is partially known, where the known part is b_0, and the unknown part is Δb. Then, Eq. (1) can be rewritten as

$$\begin{aligned} \ddot{y} &= -a_1\dot{y} - a_2 y + w + (\Delta b + b_0)u, \\ &= f + b_0 u, \end{aligned} \tag{3-2}$$

where f is the total disturbance that is composed of the system internal dynamics and the external disturbance. When taking $x_1 = y$, $x_2 = \dot{y}$, and $x_3 = f$ as state variables, its state-space representations can be expressed as:

$$\begin{aligned} \dot{x} &= Ax + Bu + E\dot{f}, \\ y &= Cx, \end{aligned} \tag{3-3}$$

where $x = \begin{pmatrix} x_1 \\ x_2 \\ x_3 \end{pmatrix}$, $\dot{x} = \begin{pmatrix} \dot{x_1} \\ \dot{x_2} \\ \dot{x_3} \end{pmatrix}$, $A = \begin{pmatrix} 0 & 1 & 0 \\ 0 & 0 & 1 \\ 0 & 0 & 0 \end{pmatrix}$, $B = \begin{pmatrix} 0 \\ b_0 \\ 0 \end{pmatrix}$, $E = \begin{pmatrix} 0 \\ 0 \\ 1 \end{pmatrix}$, and $C = (1\ 0\ 0)$.

Then, the linear ESO is created for the above state-space model:

$$\begin{pmatrix} \dot{z_1} \\ \dot{z_2} \\ \dot{z_3} \end{pmatrix} = \begin{pmatrix} 0 & 1 & 0 \\ 0 & 0 & 1 \\ 0 & 0 & 0 \end{pmatrix} \begin{pmatrix} z_1 \\ z_2 \\ z_3 \end{pmatrix} + \begin{pmatrix} 0 \\ b_0 \\ 0 \end{pmatrix} u + \begin{pmatrix} l_1 \\ l_2 \\ l_3 \end{pmatrix} (\hat{y} - z_1), \tag{3-4}$$

where $\hat{y}$ is the output, and z_1, z_2, and z_3 are the estimated values of x_1, x_2, and x_3, respectively. Then, the linear ESO can be rewritten as:

$$\dot{z} = Az + Bu + L(y - Cz),$$
$$\hat{y} = Cz, \tag{3-5}$$

where $L = \begin{pmatrix} l_1 \\ l_2 \\ l_3 \end{pmatrix}$. z_1 and z_2 are used as the feedback of the PD controller. For the disturbance rejection, z_3 is subtracted from the PD controller's output.

3.3 Cascade-ADRC with First Order LESO Attitude Controller

Due to the high accuracy and reliability of modern inertial sensors, the estimation of system outputs in LESO can be omitted. Therefore, using a reduced order LESO can reduce the massive of calculations and simplify the implementation of control algorithm.

3.3.1 Reduced order LESO

Suppose the system output y is measurable and reliable, the estimated output y is removed from the observer, keeping the estimations of $\dot{y}$ and f. Then, a second order LESO with $z = (z_1\ z_2)^T \in R^2$, where $z1$ and $z2$ are estimated values for $\dot{y}$ and f, can be written as below:

$$\dot{z} = A_2 z + B_2 u + L_2(\dot{y} - C_2 z),$$
$$\hat{f} = Vz, \tag{3-6}$$

where $A_2 = \begin{pmatrix} 0 & 1 \\ 0 & 0 \end{pmatrix}$, $B_2 = \begin{pmatrix} b_0 \\ 0 \end{pmatrix}$, $L_2 = \begin{pmatrix} l_1 \\ l_2 \end{pmatrix}$, $C_2 = (1\ 0)$, and $V = (0\ 1)$.

Furthermore, suppose y and $\dot{y}$ are both measurable and reliable, then LESO only keeps $z \in R^1$ for disturbance estimation. Thus, $\ddot{y}$ can be introduced to correct the feedback, and a first order LESO can be written as:

$$\dot{z} = A_1 z + B_1 u + L_1(\ddot{y} - b_0 u - C_1 z),$$
$$\hat{f} = z, \tag{3-7}$$

where $A_1 = (0)$, $B_1 = (0)$, $L_1 = (l_1)$, $C_1 = (1)$, and $V_1 = (1)$.

Equation (7) can be rewritten as：

$$\begin{aligned} \dot{z} &= l_1(\ddot{y} - b_0 u - Cz), \\ \hat{f} &= z. \end{aligned} \tag{3-8}$$

Observe that the calculations in LESO have been simplified to scalar calculations [55][56]. Thus, we applied the first order LESO is used to simplify the attitude controller.

3.3.2 Cascade-LADRC attitude controller with first order LESO

A conventional cascade PID attitude controller employs a PID controller for angular velocity control. However, we replaced the PID controller with LADRC (with first order LESO) and proposed the cascade LADRC controller in Fig. 3-4 and Fig.3-5 shows the LADRC attitude controller with first order LESO.

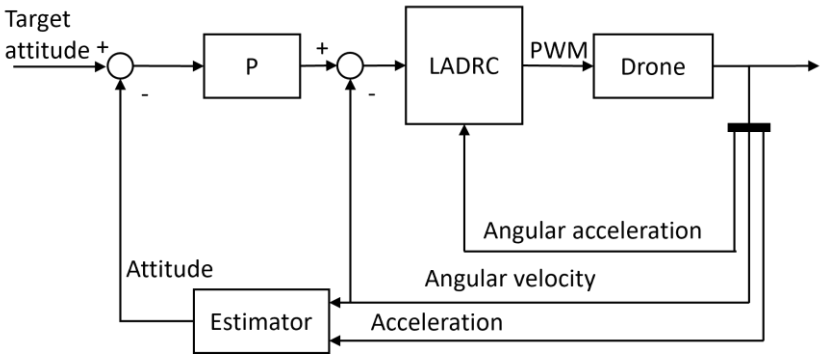

Fig.3- 4 Proposed cascade-LADRC attitude controller block diagram

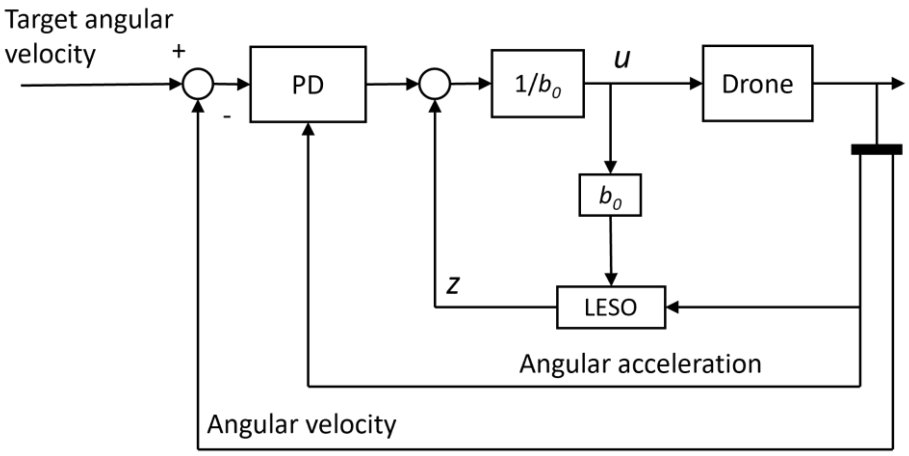

Fig.3- 5 Detailed block diagram of the LADRC in Fig. 3-4

Drone attitude angles can be calculated using an accelerometer and gyroscope. The angular velocity is measured using a gyroscope, and the angular acceleration is given as the differential of the angular velocity. Considering the roll-direction attitude control, the roll and controller parameters of a drone attitude angle are shown in Table 3-1.

Table 3- 1 Definition of drone attitude angles

Parameter	**Symbol**
Roll angle setpoint	φ_{ref}
Roll angular velocity setpoint	$\dot{\varphi}_{\mathrm{ref}}$
Measured value of roll angle	φ
Parameter P of P-Controller	kp_1
Parameter P of LADRC Controller	kp_2
Parameter D of LADRC Controller	kd_2
LADRC Controller LESO Parameter	b_0
LADRC Controller LESO Parameter	l
Controller output	u_{roll}

The inner loop input is calculated using the P controller:

$$\dot{\varphi}_{\text{ref}} = kp_1(\varphi_{\text{ref}} - \varphi\ ). \tag{3-9}$$

The first order LESO estimates the disturbance value based on:

$$\dot{z} = l_1(\ddot{\varphi} - b_0 u - z), \tag{3-10}$$

and the output of the LADRC controller is calculated using

$$u_{roll} = \frac{kp_2(\dot{\varphi}_{ref} - \dot{\varphi}) - kd_2\ddot{\varphi} - z}{b_0}. \tag{3-11}$$

The controller for other attitude angles is the same as the above equations.

3.4 Simulation

In order to evaluate the performance of the proposed method, a comparative experiment was implemented by simulation. An attitude model of a quadrotor drone was built as the control plant. By observing the response of each control method under the same disturbance, the robustness, and the disturbance-rejection performance of each method were evaluated.

3.4.1 Drone attitude model

The modeling parameters of a drone are shown in Table 3-2.

Table 3- 2 Definition of the attitude model parameters

Physical Quantity	**Symbol**
Roll	φ
Pitch	θ
Yaw	ψ
$\dot{\varphi}$	p
$\dot{\theta}$	q
$\dot{\psi}$	r
Inertia tensor	J
Inertia about body x axis	J_x
Inertia about body y axis	J_y
Inertia about body z axis	J_z
Torque φ	τ_φ

Torque θ	τ_θ
Torque ψ	τ_ψ
Length of body arm	l
Thrust of left motor	F_{left}
Thrust of right motor	F_{right}
Thrust of front motor	F_{front}
Thrust of back motor	F_{back}

When a drone has a "+" structure, the output torques generated by each two opposite motors are given [57] as:

$$\begin{aligned} \tau_\varphi &= l\left(F_{\text{left}} - F_{\text{right}}\right), \\ \tau_\theta &= l(F_{\text{front}} - F_{\text{back}}), \\ \tau_\psi &= F_{\text{left}} + F_{\text{right}} - F_{\text{front}} - F_{\text{back}}. \end{aligned} \tag{3-12}$$

Also, the attitude angular acceleration can be written by the torque equation, as shown in Eq. (13):

$$\begin{pmatrix} \dot{\varphi} \\ \dot{\theta} \\ \dot{\psi} \end{pmatrix} = -J^{-1} w \times J \begin{pmatrix} p \\ q \\ r \end{pmatrix} - J^{-1} \begin{pmatrix} \tau_\varphi \\ \tau_\theta \\ \tau_\psi \end{pmatrix}, \tag{3-13}$$

where $J = \begin{pmatrix} J_x & 0 & 0 \\ 0 & J_y & 0 \\ 0 & 0 & J_z \end{pmatrix}$, $w \times = \begin{pmatrix} 0 & -r & q \\ r & 0 & -p \\ -q & p & 0 \end{pmatrix}$.

Only when considering the roll direction and linear approximation with small q and r values, a roll-control model (Fig. 3-6) based on Eq. (3-13) is built for simulation. The system input is the torque that scaled to the PWM value, and the output is the angle in radians. The arm length of the modeled drone is 0.3 m, and the inertia about axis x is 0.002 kg/m^3.

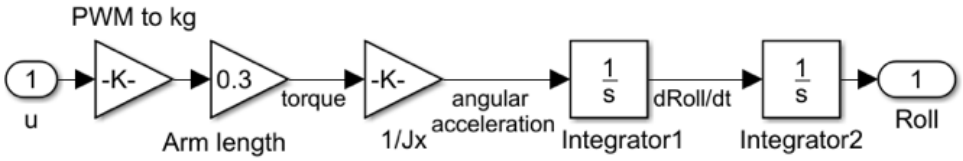

Fig.3- 6 One-dimensional simple attitude model in the simulator

3.4.2 Comparative experiment

In this section, the conventional cascade PID controller and proposed controller are implemented in the simulator (Fig.3-7, Fig.3-8):

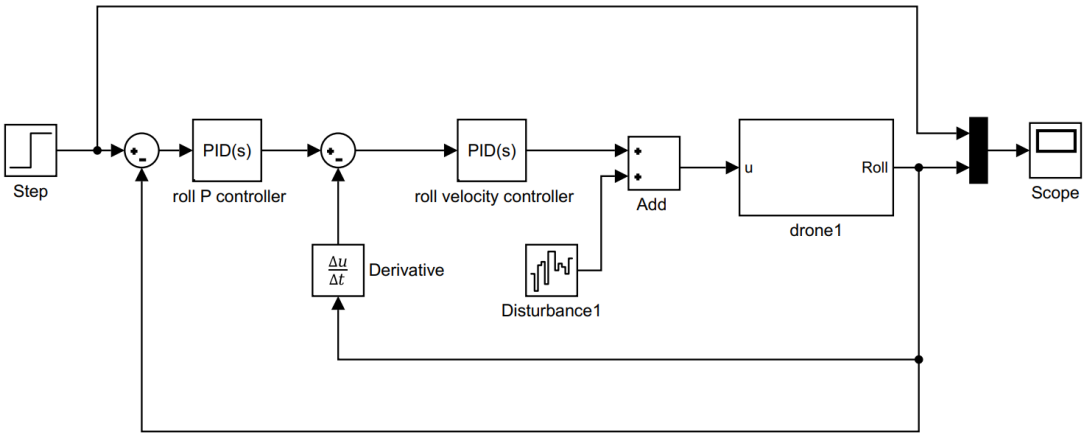

Fig.3- 7 Cascade PID controller in simulator

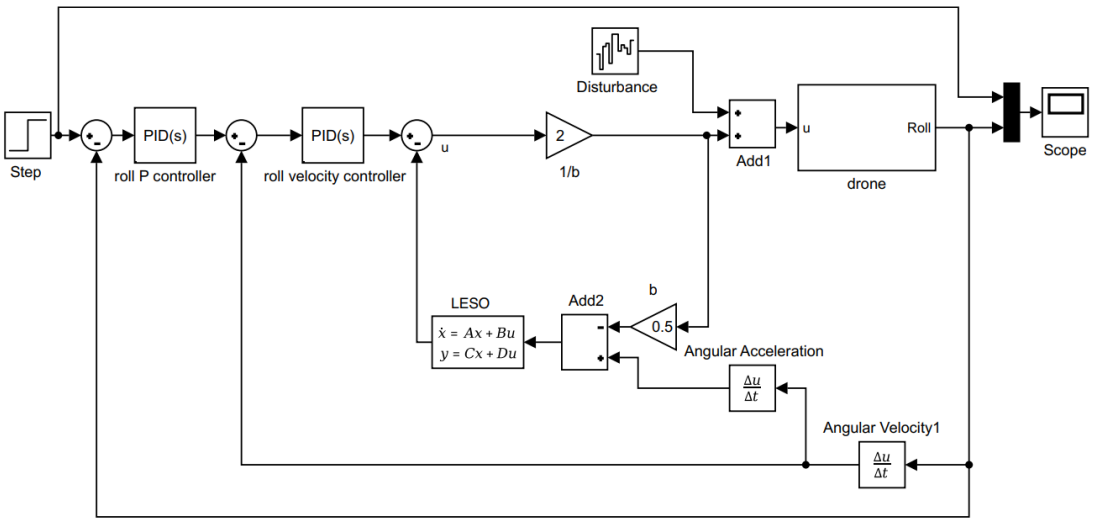

Fig.3- 8 Proposed method in simulator

The system input command and external disturbance for each method are generated by the same signal sources. The reduced order LESO is constructed by a one-dimensional state-space model. The output of each method is limited to a PWM value 20000 that means 4 kg.

First, the response to the step signal is compared. Then, the robustness under different disturbance is compared. Two kinds of disturbance signals were generated, where one is a random noise signal that simulates the wind disturbance (Fig.3-9), and the other one is a step signal (Fig. 3-10) that simulates the payload and the unbalanced situation.

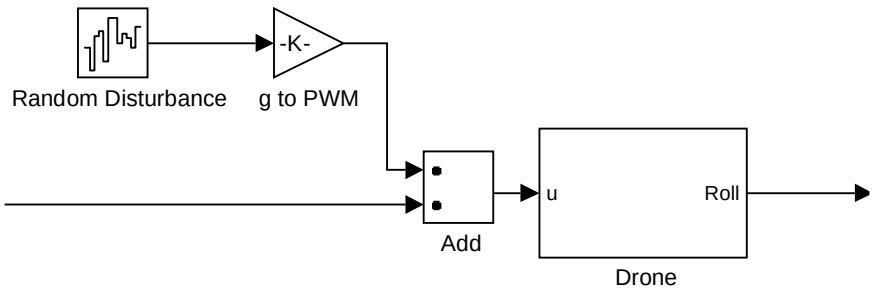

Fig.3- 9 Random disturbance in the simulator

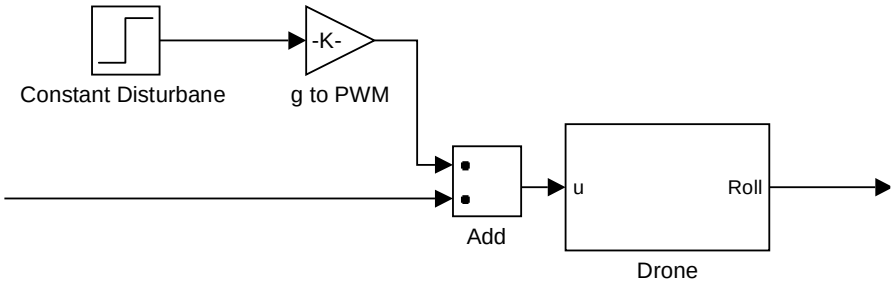

Fig.3- 10 Constant disturbance in the simulator

3.4.3 Results

Related studies[58] have demonstrated through equivalent transformations that PID is a special case of LADRC with an infinite observer bandwidth. Their frequency response at low frequencies has similar response characteristics. In this comparative experiment, we adjusted the controllers to have same PID gains. Although there is no integral term in the proposed method, from Eq.3-10 and 3-11, it is known that the integral gain of the proposed method is approximately equal to Pl_1, b_0 can be tuned. The step response of conventional and proposed controller is shown in Fig.3-11.

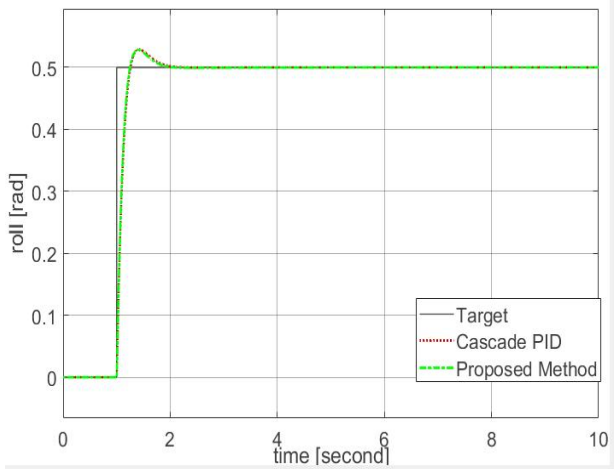

Fig.3- 11 Step response of the conventional and proposed controller

When the command signal was fixed, the performance of each system under random disturbance is shown in Fig.3-12, the random disturbance signal is shown in Fig.3-13, and the output of each controller is shown in Fig.3-14.

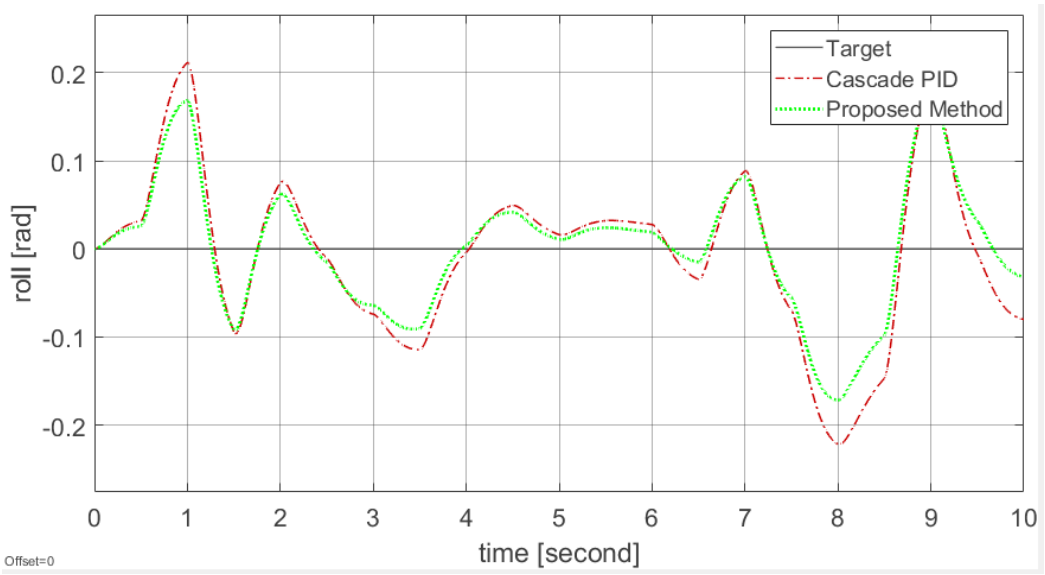

Fig.3- 12 Performance of conventional and proposed controller during the random disturbance, IAE of Cascade PID:0.679, IAE of proposed method:0.552

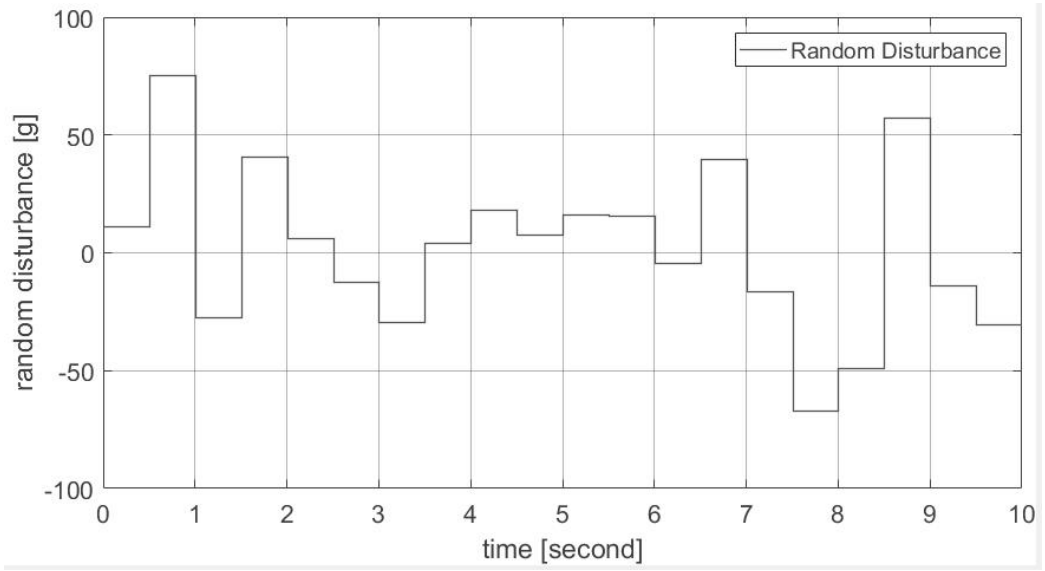

Fig.3- 13 Random disturbance signal (noise power=500, sample time=0.5s)

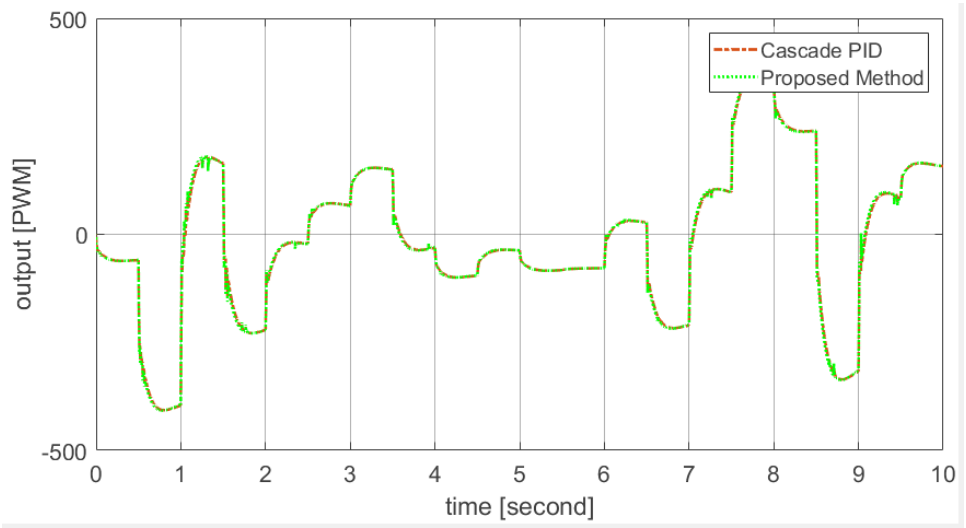

Fig.3- 14 Controller output during the random disturbance

When the command signal is fixed, a continuous constant disturbance is applied at the moment of 1 second. The simulation results of the 2 methods are shown in Fig.3-15, the constant disturbance signal is shown in Fig.3-16, and the output of each controller is shown in Fig.3-17.

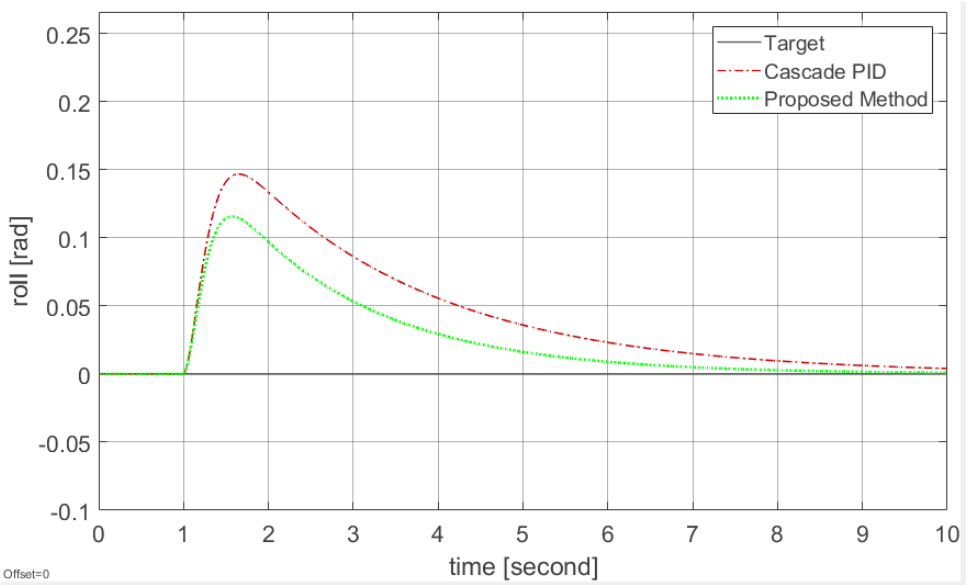

Fig.3- 15 Performance of conventional and proposed controller during the constant disturbance, IAE of Cascade PID:0.407, IAE of proposed method:0.250

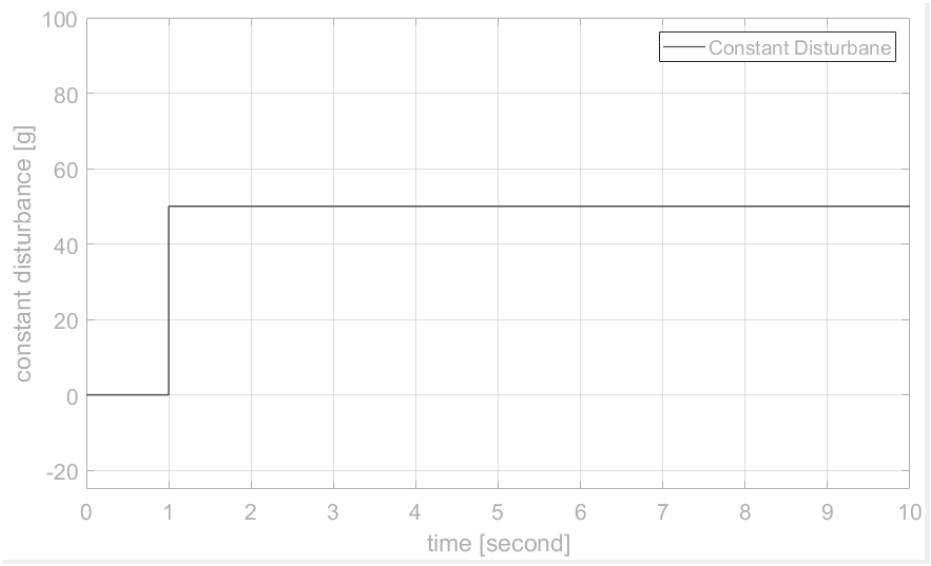

Fig.3- 16 Constant disturbance signal

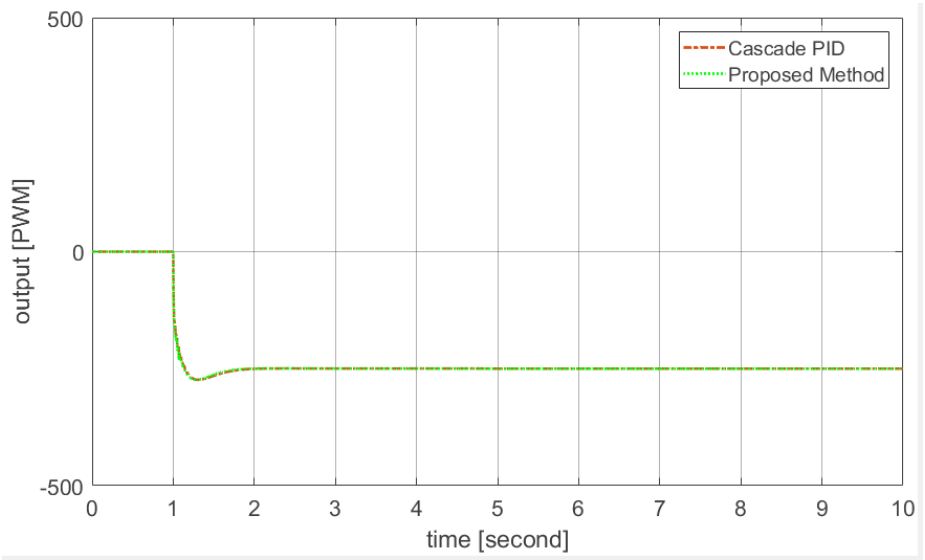

Fig.3- 17 Controller output of conventional and proposed controller during the constant disturbance

The maximum deviations under two kinds of disturbance are summarized in Table 3-3.

Table 3- 3 Maximum deviations and IAE under the random and constant disturbances

Method	Random disturbance		Constant disturbance	
	Max deviation	IAE	Max deviation	IAE
Cascade PID	0.222	0.679	0.147	0.407
Proposed Method	0.177	0.552	0.116	0.250

We integrate the error in Figure 3-12 and get IAE of the two methods, then square of outputs' L2 norm in Figure 3-14 are compared to obtain the energy consumption. It shows a 19.0% reduction in IAE when using the proposed controller. Energy consumption is only 0.22% more than conventional method. During constant disturbance, the IAE of the proposed method decreased by 38.6% under constant disturbance.

During the different disturbances, proposed method had a minimal deviation during the disturbance. These results indicate that the proposed method can effectively suppress the oscillations caused by random disturbances. During the continuous constant disturbance, the simulation provided a similar result that the proposed method has the least deviation and best convergence speed.

3.4.4. Conclusion of Simulation experiment

Since modern inertial sensors for drones have high precision, the observers in conventional LADRC methods which are used for attitude control, can be further simplified. We used a simplified first order LESO method for attitude control, where the system could reduce the calculations and make the implementation lighter in weight. Due to the responsiveness of the cascade structure and the robustness of the LADRC, the cascade-LADRC method for multi-rotor attitude control is proposed. Through simulation, the performance of the proposed method was compared with conventional cascade PID controller. Under different disturbances, the proposed method had a faster response and a smaller

deviation. Compared with the cascade PID control method, which is commonly used by flight controllers, the proposed method could effectively suppress the oscillations caused by disturbances.

Chapter 4

Implementation and Comparative Experiments

4.1 Implementation of attitude control algorithm

In this chapter, we implement the efficient cascade LADRC attitude controller proposed in chapter 3 on the compact drone proposed in chapter 2 and evaluate the control performance. Then the proposed attitude controller is evaluated on a conventional structure drone.

4.1.1 Implementation of attitude controllers

Considering the attitude in the roll direction, the finite difference method is used to discretize Eq.(3-10) and estimate the disturbance value. Then, the controller output can be updated using (3-11). The disturbance estimation and control frequencies are 250 Hz, respectively.

To compare the control performance of the proposed method with the conventional method, we implemented the widely used cascade PID control method shown in Fig. 3-2. Process of each control algorithm is shown in Table4-1 and Table 4-2.

Table 4- 1 Output update of cascade PID controller

Output Update of Cascade PID Control	
Begin	
1	$\dot{\varphi}_{\mathrm{ref}} = kp_1(\varphi_{\mathrm{ref}} - \varphi\,)$
2	$e_{\dot{\varphi}} := \dot{\varphi}_{\mathrm{ref}} - \dot{\varphi}$
3	$I_{\dot{\varphi}} :=\ ki\, e_{\dot{\varphi}}$
4	$I_{\dot{\varphi}} :=\ Limit(I_{\dot{\varphi}})$
5	$u :=\ kp_2 e_{\dot{\varphi}} + I_{\dot{\varphi}} - kd_2\ddot{\varphi}$
End	

Table 4- 2 Output update of proposed controller

Output Update of Cascade LADRC with first order LESO	
Begin	
1	$\dot{\varphi}_{\mathrm{ref}} := kp_1(\varphi_{\mathrm{ref}} - \varphi)$
2	$\dot{z} := l_1(\ddot{\varphi} - b_0 u - z)$
3	$z_t := z_{t-1} + \dot{z} \times dT$
4	$z_t = Limit(z_t)$
5	$u := \dfrac{kp_2(\dot{\varphi}_{\mathrm{ref}} - \dot{\varphi}) - kd_2\ddot{\varphi} - z_t}{b_0}$
6	$z_{t-1} \coloneqq z_t$
End	

4.1.2 Comparison of computing cost

When using a full order observer, it can be discretized using Eq. (4-1)[59], β is the full order observer bandwidth. When disregarding the time consumed on reading and preprocessing time of the data (calculation time for $\emptyset_E$, Γ_E, H_E, J_E), the comparison results of first order and full order observer computing cost are shown in Table 4-3.

$$\begin{aligned} z(k+1) &= \emptyset_E z(k) + \Gamma_E u_d(k), \\ y_d(k) &= H_E x + J_E u_d(k), \end{aligned} \tag{4-1}$$

where

$$\emptyset_E = \begin{pmatrix} 3\beta - 2 & dT & 0 \\ -3(1-\beta)^2/dT & 1 & dT \\ -(1-\beta)^3/dT^2 & 0 & 1 \end{pmatrix},\ \Gamma_E = \begin{pmatrix} 0 & 3-3\beta \\ b_0 dT & 3(1-\beta)^2/dT \\ 0 & (1-\beta)^3/dT^2 \end{pmatrix},$$

$$H_E = \begin{pmatrix} \beta^3 & 0 & 0 \\ (-2+3\beta-\beta^3)/dT & 1 & 0 \\ -(1-\beta)^3/dT^2 & 0 & 1 \end{pmatrix}, \text{and}$$

$$J_E = \begin{pmatrix} 0 & 1-\beta^3 \\ 0 & (2-3\beta-\beta^3)/dT \\ 0 & (1-\beta)^3/dT^2 \end{pmatrix}.$$

Table 4- 3 Observer calculating cost comparison of full order LESO and reduced order LESO

Observer	Addition and subtraction execution times	Multiplication execution times
Full order LESO	18	30
First order LESO	2	4

The number of addition and subtraction operations for the first order observer is 1/9 of that of the full order observer. The number of multiplication operations has also been reduced by more than 6 times.
Next, we compare the computing cost of the cascade PID and the proposed method. When disregarding the time consumed on reading and preprocessing time of the data, a full process computing cost in one loop for conventional cascade PID and proposed method are shown in Table 4-4. The number of addition and subtraction operations in proposed method is 3 more than that of cascade PID. The number of multiplication and division operations in proposed method is 2 and 1 more than that of cascade PID respectively. After implementation, the execution times for cascade PID and the proposed method are 13us and 26us respectively.

Table 4- 4 A full process calculating cost comparison of cascade PID and proposed method

Observer	Addition and subtraction execution times	Multiplication execution times	Division Multiplication execution times	Limit function operation execution times
Cascade PID	4	4	0	1
Proposed Method	7	6	1	1

4.1.3 Implementation of velocity control and position control

The velocity and position controls were implemented using the cascade control method. Their block diagrams are shown in Fig.4-1 and Fig.4-2. Since attitude control is one most essential part of the velocity and position controls, we compared the velocity and position control performances of the drone when either the proposed attitude control method or the conventional method was applied.

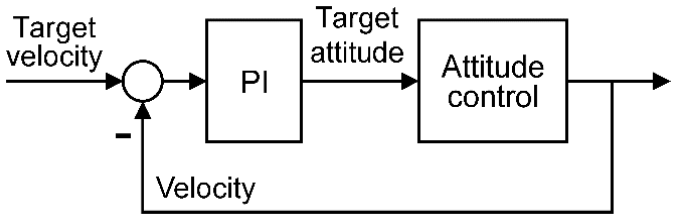

Fig.4- 1 Velocity control block diagram

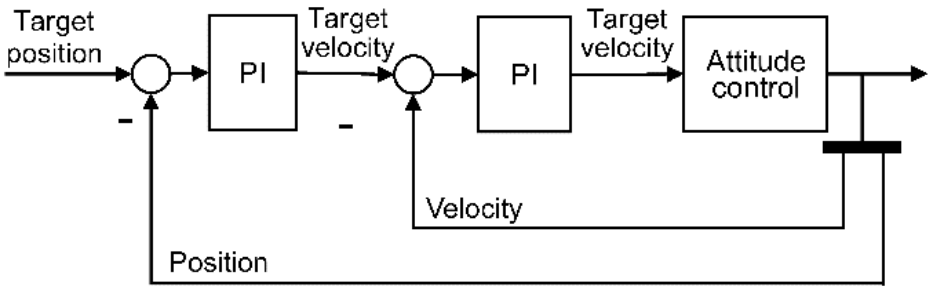

Fig.4- 2 Position Control block diagram

4.2 Performance Evaluation of Cascade LADRC Attitude Controller on Compact Structure Drone

In Chapter 2, a larger error in attitude control is shown when using the proposed compact structure.
The proposed attitude controller is therefore applied to the quadcopter with proposed compact structure. A comparative experiment with conventional cascade PID controller was performed to verify the robustness of the proposed attitude controller.

4.2.1 Comparative experiment on quadcopter with compact structure

In this comparative experiment, we compared the performance of the conventional and proposed attitude controllers when responding to the 0-degree command. The flying height was set at 1.5 m. We completed 5 sets of the comparison. Fig.4-3 and Fig.4-4 show the result of 2 controllers.

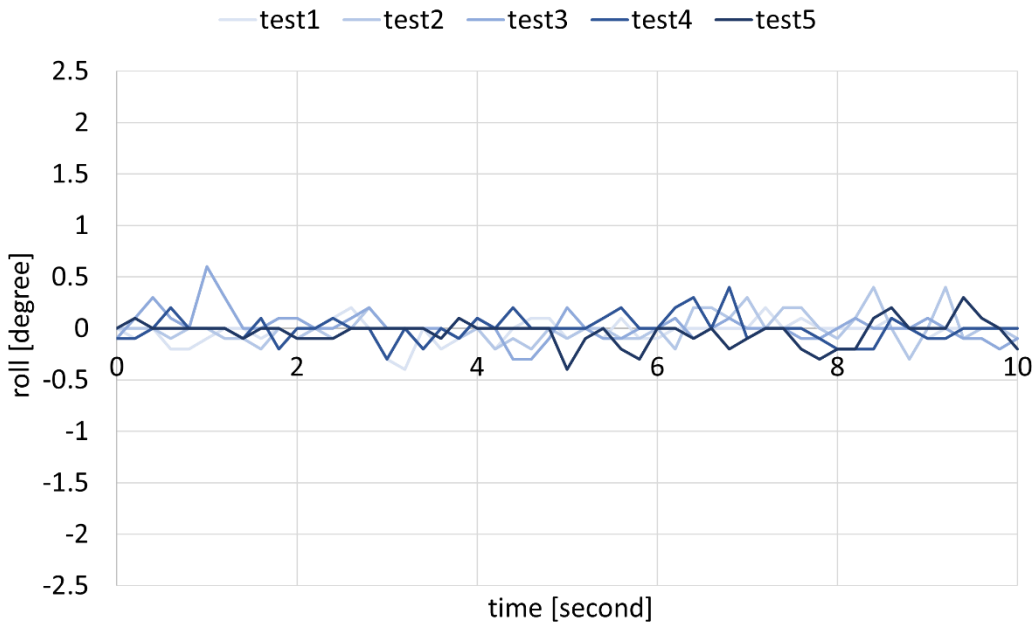

Fig.4- 3 0-degree response of cascade PID controller

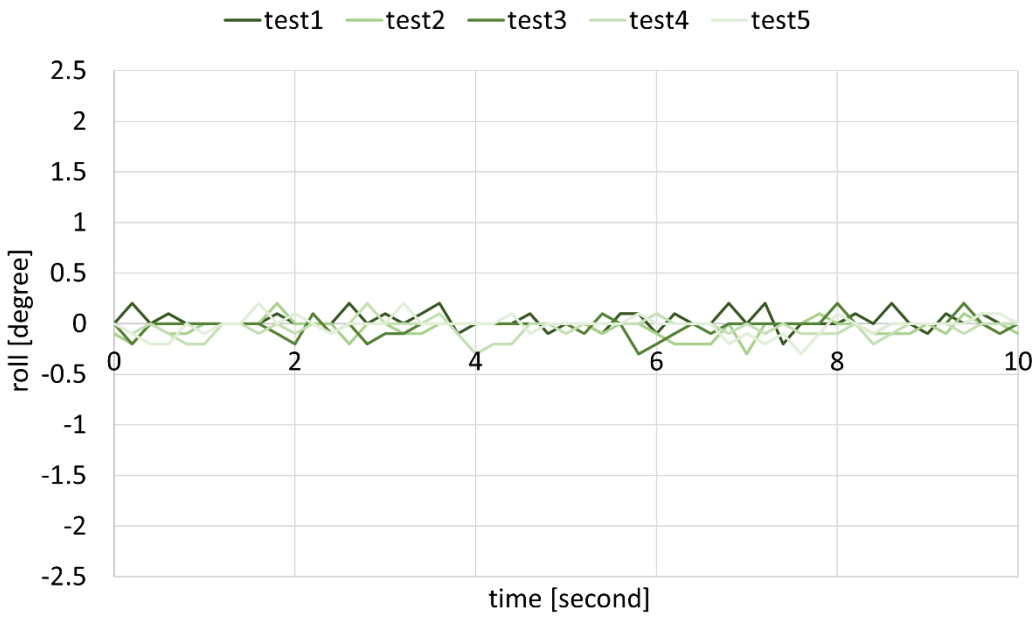

Fig.4- 4 0-degree response of cascade LADRC with reduced order observer

4.2.2 Result of comparative experiment on quadcopter with

compact structure

Table 4-5 shows the IAE in 10s of each controller. Table 4-6 shows the standard deviation in 10s of each controller.

Table 4- 5 IAE in 10s of each controller on compact structure drone

Method	IAE				
	Test1	Test2	Test3	Test4	Test5
Proposed	3.0	3.1	2.9	2.6	2.9
Cascade PID	4.5	4.1	3.9	4.9	3.6

Table 4- 6 Standard deviation of each controller on compact structure drone

Method	Standard deviation				
	Test1	Test2	Test3	Test4	Test5
Proposed	0.087	0.089	0.087	0.089	0.094
Cascade PID	0.143	0.128	0.121	0.143	0.109

The proposed controller shows a smaller deviation, with a smaller IAE in 10 seconds than the cascade PID controller. The IAE in 10 seconds was reduced by 30%, demonstrates that the proposed controller can achieve more robust control on the drone with compact structure.

4.3 Implementation of a vision-based drone

We designed and built a vision-based compact quad-rotor drone to test the control algorithm. In the basic control, a 72 MHz microcontroller was used as the flight controller to perform attitude calculation, control, and data communication. For Realsense T200 series cameras are widely used in robot indoor applications [60][61][62]. In our research, the internal module t261 of t265 was used for obtaining real-time information on the velocity, position, and orientation of the drone. A Raspberry Pi 4 is used as the high-level controller to complete the data communication with the

flight controller. The specifications of the implemented drone are shown in Table 4-7. The schematic of drone's hardware system is shown in Fig.4-5 and the implemented drone is shown in Fig.4-6 .

Table 4- 7 Specifications of the implemented drone

Dimensions	399.8 × 294.6 × 16.9 mm
Battery	3cell LiPo battery
Propeller	7 × 2.7inch
Motor	2305KV brushless motor
Flight controller IC	STM32F103C8T6
High-level controller	Raspberry PI 4
Tracking camera	Realsense T261
IMU sensor	MPU6050

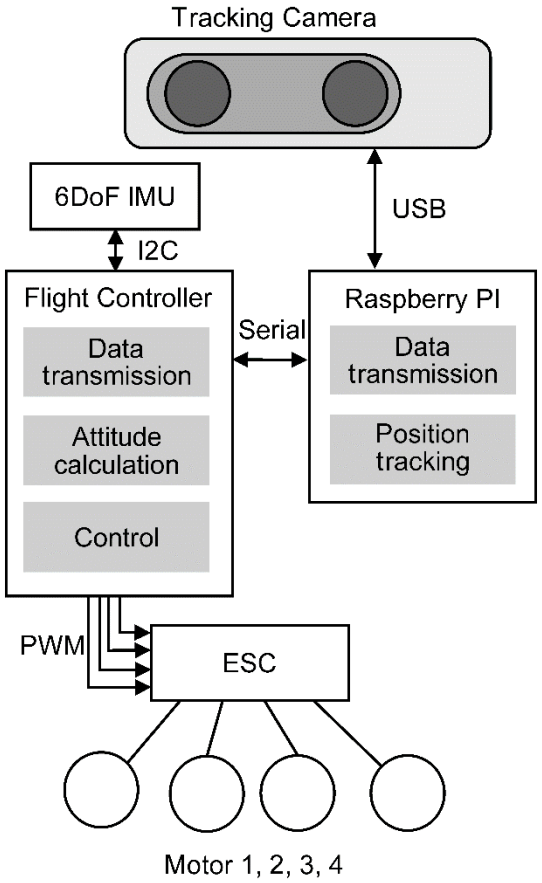

Fig.4- 5 Schematic of the drone's hardware system

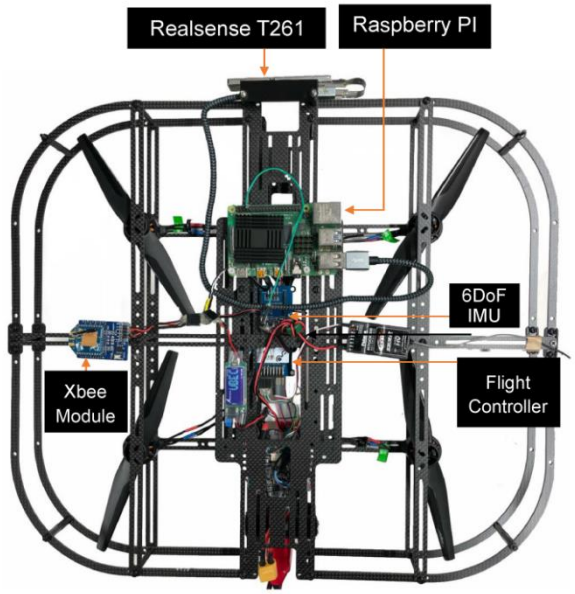

Fig.4- 6 Implemented drone

The estimation of attitude angle pitch and roll uses a complementary

filter [63]. The data of the position, velocity, and direction angle obtained from the high-level controller are transmitted to the flight controller at a frequency of 10 Hz to perform velocity, position, and yaw control. Concurrently, the ground station collects flight data at a frequency of 5 Hz.

4.4 Comparative Experiments

Since attitude control is a basic part of the velocity and position controls for multi-rotor drones, indoor flight experiments were conducted to compare the proposed control method with the conventional cascade PID. Furthermore, the performance of the velocity and position controls was compared for the two attitude control methods, respectively.

4.4.1. Attitude Control Comparative Experiment

In the attitude control comparative experiment, we compared the performance of the conventional attitude and proposed attitude controls when responding to the same commands. The flying height was set at 1.5 m. The same PD parameters were used in the conventional cascade PID and the proposed method of the controller. The attitude command is a step signal from 0°–5°, and we completed 5 sets of steps comparison. Fig.4-7 and Fig.4-8 show examples of posture comparison experiments.

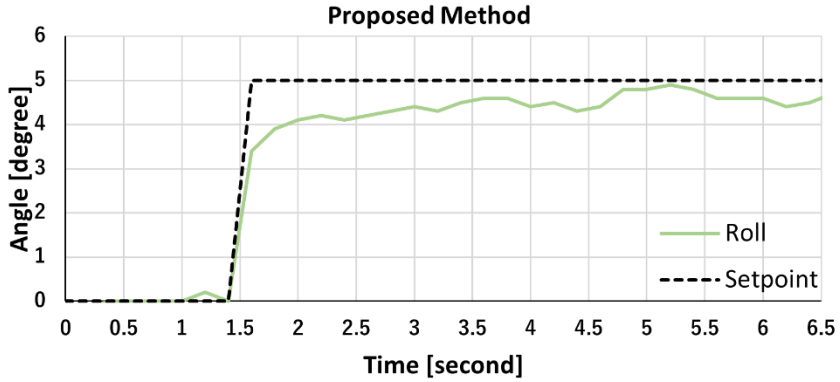

Fig.4- 7 Example of attitude response when using a cascade LADRC with reduced order LESO as an attitude controller

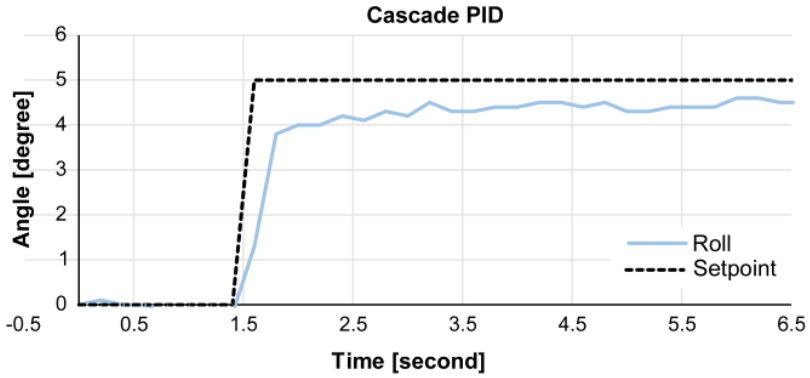

Fig.4- 8 Example of attitude response when using a cascade PID as an attitude controller

These two control methods were evaluated by comparing the IAE of the 5 experimental sets. The IAE and average error of the 5 sets of tests are shown in Table 4-8 and Table 4-9.

Table 4- 8 IAE of proposed control method and conventional method in attitude comparative experiments

Method	IAE				
	Test1	Test2	Test3	Test4	Test5
Proposed	3.02	3.02	3.8	2.96	3.44
Cascade PID	3.26	4.24	3.46	4.06	3.68

Table 4- 9 Average IAE of 5 sets of tests

Method	Average IAE of each method
Proposed	3.25
Cascade PID	3.74

The results of the attitude control comparison show that compared with the conventional cascade PID attitude control method, the proposed method has a smaller cumulative error. Steady-state errors in 2 methods

can be caused by sensor offsets

4.4.2. Velocity Control Comparative Experiment

In the velocity control comparison experiment, the flying height was set at 1.5 m. The velocity command is a step signal from 0–50 cm/s. We compared the performance of the step response for the conventional and proposed methods as attitude controllers. The block diagram of the velocity and attitude controls is shown in Fig.4-1. considering the velocity control in the left-right direction, we did 5 sets of step response comparison. Fig.4-9 and Fig.4-10 show examples of velocity comparison experiments.

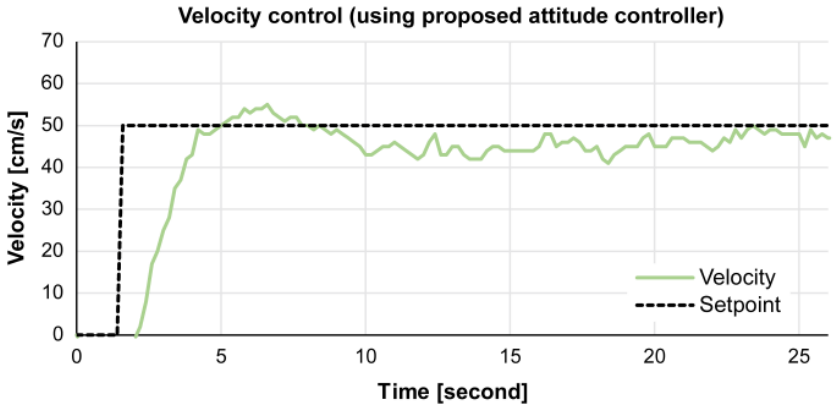

Fig.4- 9 Example of velocity response when using a cascade LADRC with reduced order LESO as attitude controller

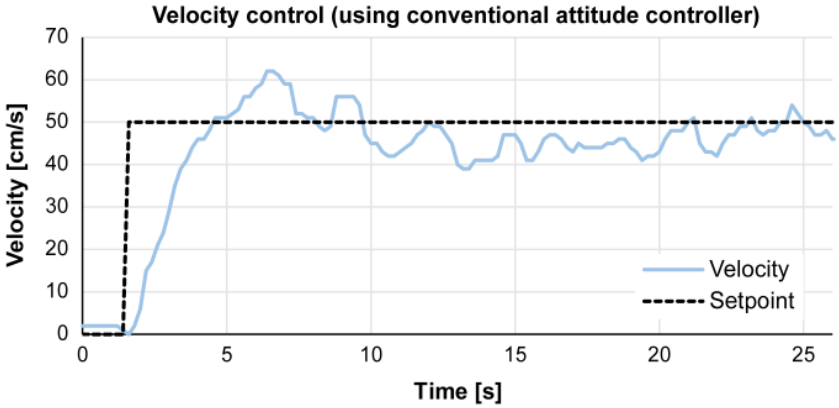

Fig.4- 10 Example of velocity response when using a cascade PID as

attitude controller

Next, we evaluate the control effect by comparing the overshoot, peak time, and IAE of the 5 datasets. The overshoot and average overshoot of the 5 test sets are shown in Table 4-10 and Table 4-11.

Table 4- 10 Example of velocity response when using a cascade PID as attitude controller

Method	Overshoot [cm/s]				
	Test1	Test2	Test3	Test4	Test5
Proposed	5	7	11	8	9
Cascade PID	12	7	11	8	13

Table 4- 11 Example of velocity response when using a cascade PID as attitude controller

Method	Average overshoot for each method
Proposed	8.0
Cascade PID	10.2

The peak and average peak times of the five experiments are shown in Table 4-12 and Table 4-13.

Table 4- 12 Peak time of velocity response when using the proposed and conventional methods as attitude controller

Method	Peak time [s]				
	Test1	Test2	Test3	Test4	Test5
Proposed	6.6	4.2	6.6	6.6	6.2
Cascade PID	6.4	6.0	7.4	6.8	6.2

Table 4- 13 Average peak time of velocity response when using the proposed and conventional methods as attitude controller

Method	Average peak time of each method
Proposed	6.04
Cascade PID	6.56

The IAE and average IAE of the 5 test sets are shown in Table 4-14 and Table 4-15.

Table 4- 14 15–43 s velocity IAE for the proposed and conventional methods as attitude controller

Method	IAE from 9s to 26s				
	Test1	Test2	Test3	Test4	Test5
Proposed	77.6	59.4	70.8	65.6	65.8
Cascade PID	80.6	65.6	80.4	70.0	53.8

Table 4- 15 Average IAE for the proposed and conventional methods as attitude controller

Method	Average IAE of each method
Proposed	67.84
Cascade PID	70.08

The results from the velocity control comparison show that compared with using cascade PID as attitude control, the proposed attitude controller produced velocity responses with lower overshoot, faster speed, and smaller IAE.

4.4.3. Position Control Comparison Experiment

For the position control comparison experiment, we compared the hovering performance for the conventional and proposed methods as attitude controllers. To test the performance of the controllers in windy and no-wind environments, a fan was used as a disturbance generator 1 m from the drone. The experimental environment is shown in Fig.4-11.

Considering the position control of the body coordinate in the left and right directions, the block diagram of the position, velocity control, and attitude controllers are shown in Fig.4-2. The velocity and attitude controllers were used in chapter 5.2. The drone flies at a height of 0.5 m. When the electric fan is off, the hovering data of the drone in 73 s is shown in Fig.4-12. When the fan is started, the wind speed at 1m from the drone is about 1.3m/s (measured by an air-speedometer). Fig.4-13 shows the hovering data of the drone in 73 s under wind disturbance.

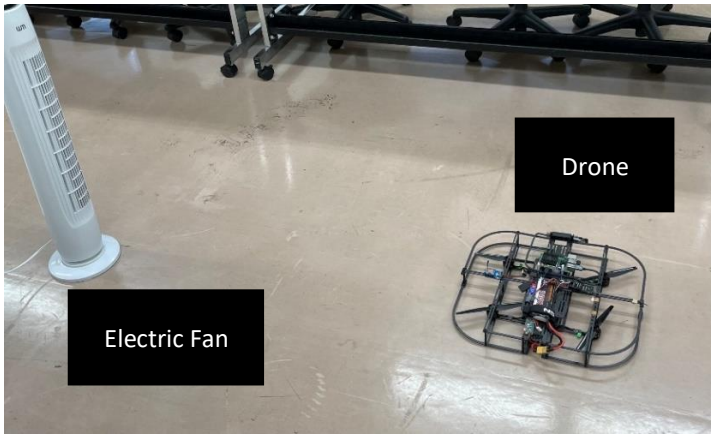

Fig.4- 11 Indoor experimental environment for position control experiments

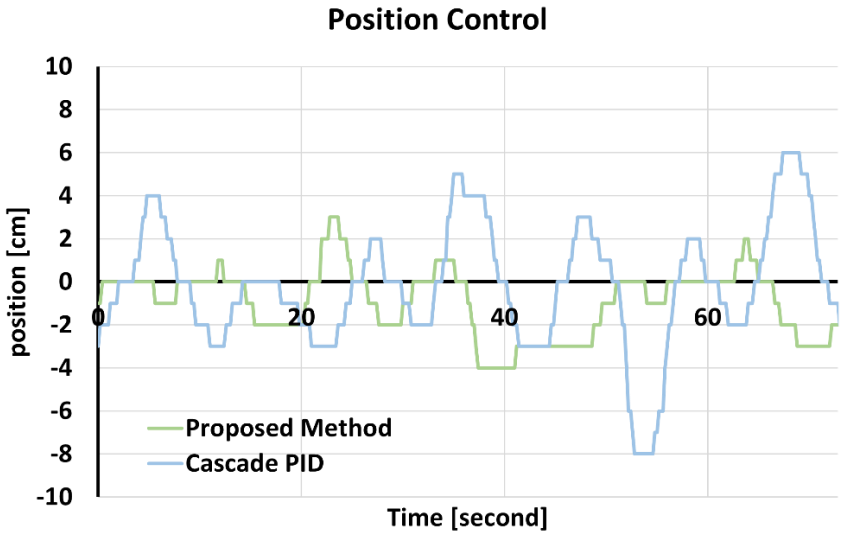

Fig.4- 12 Hovering performance for the proposed and conventional methods as attitude controller

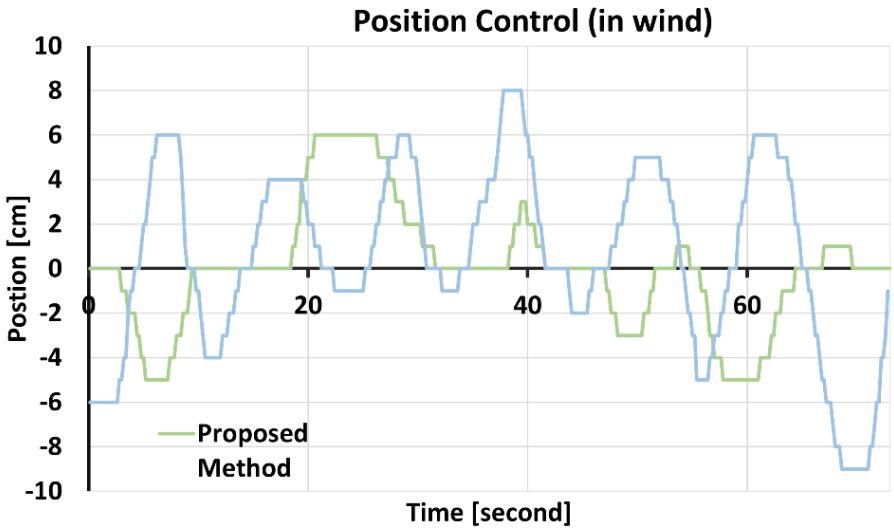

Fig.4- 13 Hovering performance under wind disturbance for the proposed and conventional methods as attitude controller

The control effect is evaluated by comparing the maximum deviation, standard deviation, and IAE within 73s. The maximum deviation, standard deviation, and cumulative error from the experiment are shown in Table 4-16, Table 4-17, and Table 4-18.

Table 4- 16 Maximum deviation during the hovering tests

Method	Maximum deviation [cm]	
	No disturbance	Wind
Proposed	4	6
Cascade PID	8	9

Table 4- 17 Maximum deviation during the hovering tests

Method	Standard deviation	
	No disturbance	Wind
Proposed	1.28	2.72
Cascade PID	1.91	4.12

Table 4- 18 IAE of each method during hovering tests

Method	IAE	
	No disturbance	Wind
Proposed	93.0	127.2
Cascade PID	152.4	221.8

Results of the position control comparison show that compared with using cascade PID as attitude control, using the proposed attitude controller produces a smaller deviation. Furthermore, under the no-wind and wind conditions, IAE reduced by 39.0% and 42.7%, respectively.

4.4.4 Conclusion of comparative experiment

To evaluate the cascade LADRC with the reduced order LESO attitude controller, we applied it to the quadcopter with proposed compact

structure. A comparative experiment with conventional cascade PID controller was performed to verify the robustness of the proposed attitude controller. The proposed controller shows a smaller deviation, with a smaller IAE than the cascade PID, demonstrates that the proposed controller can achieve more robust control on the drone with proposed compact structure. Then, we built a compact quad-rotor drone and compared the performance when using conventional attitude controller and proposed controller. Results of the velocity control comparison show that the velocity responds faster with lower overshoot and smaller IAE when the proposed attitude controller is used. The experimental results of position control comparison show that the deviation during hovering is smaller, and the performance is more stable under the interference of wind when the proposed attitude controller is used.

References

[1]. B. Canis, Unmanned Aircraft Systems (UAS): Commercial Outlook for a New Industry, Washington, DC: Congressional Research Service, 2015

[2]. Consumer Drones Global Market Report 2021: COVID 19 Growth And Change to 2030, The Business Research Company, 2021

[3]. https://www.gminsights.com/pressrelease/unmanned-aerial-vehicles-UAV-commercial-drone-market

[4]. Mishra, Balmukund & Garg, Deepak & Narang, Pratik & Mishra, Vipul. (2020). Drone-surveillance for search and rescue in natural disaster. Computer Communications. 156. 10.1016/j.comcom.2020.03.012.

[5]. Schweier, Christine & Markus, Michael. (2006). Classification of Collapsed Buildings for Fast Damage and Loss Assessment. Bulletin of Earthquake Engineering. 4. 177-192. 10.1007/s10518-006-9005-2.

[6]. Restas, Agoston. (2015). Drone Applications for Supporting Disaster Management. World Journal of Engineering and Technology. 03. 316-321. 10.4236/wjet.2015.33C047.

[7]. Ruggles, Samantha & Clark, Joseph & Franke, Kevin & Wolfe, Derek & Reimschiissel, Brandon & Martin, Abe & Okeson, Trent & Hedengren, John. (2016). Comparison of SfM Computer Vision Point Clouds of a Landslide Derived from Multiple Small UAV Platforms and Sensors to a TLS based Model. Journal of Unmanned

Vehicle Systems. 4. 10.1139/juvs-2015-0043.

[8]. Palmer, Logan & Franke, Kevin & Martin, Abe & Sines, Brendan & Rollins, Kyle & Hedengren, John. (2015). Application and Accuracy of Structure from Motion Computer Vision Models with Full-Scale Geotechnical Field Tests. Geotechnical Special Publication. 2432-2441. 10.1061/9780784479087.225.

[9]. Franke, Kevin & Rollins, Kyle & Ledezma, Christian & Hedengren, John & Wolfe, Derek & Ruggles, Samantha & Bender, Christopher & Reimschiissel, Brandon. (2016). Reconnaissance of Two Liquefaction Sites Using Small Unmanned Aerial Vehicles and Structure from Motion Computer Vision Following the April 1, 2014 Chile Earthquake. Journal of Geotechnical and Geoenvironmental Engineering. 143. 04016125. 10.1061/(ASCE)GT.1943-5606.0001647.

[10]. Al-Kaff, Abdulla & Moreno, Francisco Miguel & San José, Luis & Garcia, Fernando & Martín Gómez, David & de la Escalera, Arturo & Nieva, Alberto & Garcéa, José. (2017). VBII-UAV: Vision-Based Infrastructure Inspection-UAV. 221-231. 10.1007/978-3-319-56538-5_24.

[11]. Banic, Milan & Miltenovic, Aleksandar & Pavlović, Milan & Ćirić, Ivan. (2019). INTELLIGENT MACHINE VISION BASED RAILWAY INFRASTRUCTURE INSPECTION AND MONITORING USING UAV. Facta Universitatis, Series: Mechanical Engineering. 17. 357. 10.22190/FUME190507041B.

[12]. Veroustraete, Frank. (2015). The Rise of the Drones in Agriculture. EC Agridulture. 2.

[13]. Mogili, Umamaheswara & Deepak, B.. (2018). Review on Application of Drone Systems in Precision Agriculture. Procedia

Computer Science. 133. 502-509. 10.1016/j.procs.2018.07.063.

[14]. Anthony, David & Elbaum, S. & Lorenz, Aaron & Detweiler, Carrick. (2014). On crop height estimation with UAVs. IEEE International Conference on Intelligent Robots and Systems. 4805-4812. 10.1109/IROS.2014.6943245.

[15]. Guo, Wei & Carroll, Matthew & Singh, Arti & Swetnam, Tyson & Merchant, Nirav & Sarkar, Soumik & Singh, Asheesh & Ganapathysubramanian, Baskar. (2021). UAS-Based Plant Phenotyping for Research and Breeding Applications. Plant Phenomics. 2021. 1-21. 10.34133/2021/9840192.

[16]. Kingston, Derek & Beard, Randal & McLain, Tim & Larsen, Michael & Ren, Wei. (2005). Autonomous Vehicle Technologies for Small Fixed Wing UAVs. Journal of Aerospace Computing, Information, and Communication. 2. 92-108. 10.2514/6.2003-6559.

[17]. Everaerts, Jurgen. (2008). The use of unmanned aerial vehicles (UAVs) for remote sensing and mapping. The International Archives of the Photogrammetry, Remote Sensing and Spatial Information Sciences. 37.

[18]. Tang, Qing & Zhang, Ruirui & Chen, Liping & Xu, Gang & Deng, Wei & Ding, Chenchen & Xu, Min & Yi, Tongchuan & Yao, Wen & Li, Longlong. (2020). High-accuracy, high-resolution downwash flow field measurements of an unmanned helicopter for precision agriculture. Computers and Electronics in Agriculture. 173. 105390. 10.1016/j.compag.2020.105390.

[19]. Ehsani, R., Sankaran, S., Maja, J. M., & Neto, J. C. (2012). Affordable multi-rotor remote sensing platform for applications in precision horticulture. In Proc. 11th Int. Conf. Precision Agriculture, July (pp. 15-18).

[20]. Singhal, Gaurav & Bansod, Babankumar & Mathew, Lini. (2018). Unmanned Aerial Vehicle Classification, Applications and Challenges: A Review. 10.20944/preprints201811.0601.v1.

[21]. Send, W. & Fischer, M. & Jebens, K. & Mugrauer, R. & Nagarathinam, A. & Scharstein, F.. (2012). Artificial hinged-wing bird with active torsion and partially linear kinematics. 28th Congress of the International Council of the Aeronautical Sciences 2012, ICAS 2012. 2. 1148-1157.

[22]. Festo. BionicOpter. http://www.festo.com/cms/en_corp/13165.html, 2013. Accessed: 18/08/2014

[23]. Keennon, Matthew & Klingebiel, Karl & Won, Henry. (2012). Development of the Nano Hummingbird: A Tailless Flapping Wing Micro Air Vehicle. Proceedings of 50th AIAA Aerospace Sciences Meeting Including the New Horizons Forum and Aerospace Exposition. 10.2514/6.2012-588.

[24]. Wood, Robert. (2008). The First Takeoff of a Biologically Inspired At-Scale Robotic Insect. Robotics, IEEE Transactions on. 24. 341 - 347. 10.1109/TRO.2008.916997.

[25]. Ma, Kevin & Chirarattananon, Pakpong & Fuller, Sawyer & Wood, Robert. (2013). Controlled Flight of a Biologically Inspired, Insect-Scale Robot. Science (New York, N.Y.). 340. 603-7. 10.1126/science.1231806.

[26]. Li, Bai & Zhu, Yi & Wang, Zhanyong & Li, Chao & Peng, Zhong-Ren & Ge, Lixin. (2018). Use of Multi-Rotor Unmanned Aerial Vehicles for Radioactive Source Search. Remote Sensing. 10. 1-13. 10.3390/rs10050728.

[27]. Alghamdi, Yousef & Munir, Arslan & La, Hung. (2021). Architecture, Classification, and Applications of Contemporary Unmanned Aerial Vehicles. IEEE Consumer Electronics Magazine. PP. 1-1. 10.1109/MCE.2021.3063945.

[28]. Brandt, Steven. (2018). Small UAV Design Development and Sizing. 10.1007/978-3-319-32193-6_83-2.

[29]. Ozdemir, Ugur & Aktas, Yucel & Vuruskan, Aslihan & Dereli, Yasin & Tarhan, Farabi & Demirbag, Karaca & Erdem, Ahmet & Kalaycioglu, Ganime & Ozkol, Ibrahim & Inalhan, Gokhan. (2014). Design of a commercial hybrid VTOL UAV system. Journal of Intelligent & Robotic Systems. 74. 10.1007/s10846-013-9900-0.

[30]. AUVSI. (2016). The first 1000 commercial UAS exemptions. Association for Unmanned Vehicle Systems International, Unmanned Systems magazine.

[31]. https://www.parrot.com/en

[32]. https://www.dji.com/

[33]. Giernacki, Wojciech & Bondyra, Adam & Gardecki, Stanislaw & Gąsior, Przemysław. (2016). Performance of Coaxial Propulsion in Design of Multi-rotor UAVs. 10.1007/978-3-319-29357-8_46.

[34]. Torres-Sánchez, J., F. López-Granados, N. Serrano and O. Arquero (2015) High-Throughput 3-D Monitoring of Agricultural-Tree Plantations with Unmanned Aerial Vehicle (UAV) Technology, PLoS One, 10(6): e0130479.

[35]. Shelley, A. V. (2016) A Model of Human Harm from a Falling Unmanned Aircraft: Implications for UAS Regulation, International Journal of Architecture, Arts and Applications, 3(3): Article1.

[36]. https://store.dji.com/jp/product/phantom-4-pro-propeller-guard

[37]. Ohno, K., Okada, Y., Hashirama, S. and Yokoe, M. (2017) unmanned aerial vehicle for supporting close visual inspection of bridges, Journal of the Japan Society of Precision Engineering, 88(12):1066–1070.

[38]. Agrawal, K. and P. Shrivastav (2015) Multi-rotors: A Revolution In Unmanned Aerial Vehicle, International Journal of Science and Research, 4(11):1800–1804.

[39]. Yoon, S., P. Diaz, D. Boyd, W. Chan and C. Theodore (2017) Computational Aerodynamic Modeling of Small Quadcopter Vehicles, Proceedings of the AHS 73rd Annual Forum.

[40]. Ajmera, J. and V. Sankaranarayanan (2016) Point-to-Point Control of a Quadrotor: Theory and Experiment, International Federation of Automatic Control-PapersOnLine, 49-1:401–406.

[41]. Chovancová, A., T. Fico, L. Chovanec and P. Hubinsk (2014) Mathematical Modelling and Parameter Identification of Quadrotor (a survey), Procedia Engineering, 96(2014):172–181.

[42]. "Aeronautical Engineering Course, Volume 6, Propellers, 3rd Edition", Japan Aeronautical Engineers' Association Publication (in Japanese), 1–17 pp.

[43]. P. Gasior et al., “Cascade control algorithms of position and attitude for multirotor UAV”, 22nd MMAR”, pp. 47-52, 2017.

[44]. F, Lin, “Analysis and verification of multi-rotors attitude control algorithms in Pixhawk”, p. ICADME2016, 2017.

[45]. J. Han, “Active Disturbance Rejection Controller and Its Applications (in Chinese)”, Control and Decision, Vol. 13, no. 1, pp. 19-23, 1998.

[46]. J. Han, “From PID to Active Disturbance Rejection Control”, IEEE Transactions on Industrial Electronics, Vol. 56, no. 3, pp. 900-906, 2009.

[47]. Z. Gao, “Scaling and Bandwidth-Parameterization Based Controller Tuning” in Proc. Am control conference, Denver, CO, USA, pp. 4989-4996, 2003.

[48]. Y. Shan, S. Wang, A. Konvisarova and Y. Hu, “Attitude Control of Flying Wing UAV Based on Advanced ADRC”, IOP Conference Series: Materials Science and Engineering, Vol. 677, no. 5, pp. 052075, 2019.

[49]. L. Lin, C. Chen, K. Su, B. Chen and H. Li, “Design of Anti-Interference System for Fully Autonomous UAV Based on ADRC-EKF Algorithm”, 2019 2nd International Conference on Electronics and Communication Engineering (ICECE), IEEE, pp. 428-433, 2019. doi: 10.1109/ICECE48499.2019.9058559.

[50]. M. Wang, J. Qi, J. Kang, C. Wu and Z. Wang, “Rotorcraft Aerial Manipulator Control Based on Improved ADRC”, 2020 39th Chinese Controlled Conference, CCC, pp. 6744-6749, doi:

10.23919/CCC50068.2020.9188672.

[51]. Z. Zang et al., “The Design of Height Control System of Fully Autonomous UAV Based on ADRC-PID Algorithm”, Journal of Physics: Conference Series, Vol. 1650, no. 5, 2020.

[52]. X. Liang, J. Li and F. Zhao, “Attitude Control of Quadrotor UAV Based on LADRC Method”, Vol. 2019, pp. 1924-1929, 2019. doi: 10.1109/CCDC.2019.8832546.

[53]. H. Liang et al., “ADRC vs LADRC for Quadrotor UAV with Wind Disturbances”, Proc. 38th Chinese control conference, pp. 8037-8043, 2019.

[54]. W. Tan and C. Fu, “Linear Active Disturbance Rejection Control: Analysis and Tuning via IMC”, IEEE Transactions on Industrial Electronics, Vol. 65, no. 4, 2016.

[55]. G. Tian, “Reduced-order extended state observer and frequency response analysis”, Cleveland State University, 2007.

[56]. Pawar, S. N., Chile, R. H., & Patre, B. M. (2017). Modified reduced order observer based linear active disturbance rejection control for TITO systems. ISA transactions, 71, 480-494.

[57]. G. Ferrarese et al., “Modeling and Simulation of a Quad-Tilt Rotor Aircraft”, IFAC Proc., pp. 64–70, 2013.

[58]. Jin, Huiyu & Song, Jingchao & Lan, Weiyao & Gao, Zhiqiang. (2020). On the characteristics of ADRC: a PID interpretation. Science China Information Sciences. 63. 10.1007/s11432-018-9647-

6.

[59]. R. Miklosovic, A. Radke and Zhiqiang Gao, "Discrete implementation and generalization of the extended state observer," *2006 American Control Conference*, 2006, pp. 6 pp.-, doi: 10.1109/ACC.2006.1656547.

[60]. A. Alapetite, Z. Wang, J.P. Hansen, M. Zajączkowski and M. Patalan, Comparison of Three Off-the-Shelf Visual Odometry Systems, Robotics, Vol. 9, no. 3, p. 56, 2020.

[61]. J. Bayer and J. Faigl, “On Autonomous Spatial Exploration with Small Hexapod Walking Robot Using Tracking Camera Intel RealSense T265”, 2019 European Conference on Mobile Robots (ECMR), pp. 1-6, 2019. doi: 10.1109/ECMR.2019.8870968.

[62]. D. Kim et al., “Vision Aided Dynamic Exploration of Unstructured Terrain with a Small-Scale Quadruped Robot”, 2020 IEEE International Conference on Robotics and Automation (ICRA), pp. 2464-2470, 2020. doi: 10.1109/ICRA40945.2020.9196777.

[63]. M. Euston, P. Coote, R. Mahony, J. Kim and T. Hamel, “A complementary filter for attitude estimation of a fixed-wing UAV,” 2008 IEEE/RSJ International Conference on Intelligent Robots and Systems, pp. 340-345, 2008. doi: 10.1109/IROS.2008.4650766.